Journal Pre-proof

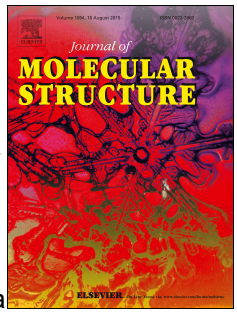

Investigation on spectra (UV–Vis, vibrational, NMR, HRMS), electronic structure (DFT calculations), molecular docking and antidiabetic activity of N-((benzo[*d*]thiazol-2-ylthio)methyl)-N-cyclohexylcyclohexanamine – A Mannich base

Krishnan Sarojini Devi, Palaniappan Subramani, Namadevan Sundaraganesan, Maria Susai Boobalan, Dhanapal Tamilvendan

PII: S0022-2860(20)30929-7

DOI: https://doi.org/10.1016/j.molstruc.2020.128604

Reference: MOLSTR 128604

To appear in: *Journal of Molecular Structure*

Received Date: 5 January 2020

Revised Date: 2 June 2020

Accepted Date: 2 June 2020

Please cite this article as: K.S. Devi, P. Subramani, N. Sundaraganesan, M.S. Boobalan, D. Tamilvendan, Investigation on spectra (UV–Vis, vibrational, NMR, HRMS), electronic structure (DFT calculations), molecular docking and antidiabetic activity of N-((benzo[*d*]thiazol-2-ylthio)methyl)-N-cyclohexylcyclohexanamine – A Mannich base, *Journal of Molecular Structure* (2020), doi: https://doi.org/10.1016/j.molstruc.2020.128604.

Krishnan Sarojini Devi: Conceptualization, Data curation Methodology, writing- Original draft preparation, Investigation

Palaniappan Subramani : Supervision

Namadevan Sundaraganesan : Software

Maria Susai Boobalan : writing- Reviewing and Editing

Dhanapal Tamilvendan : Visualization

Graphical Abstract

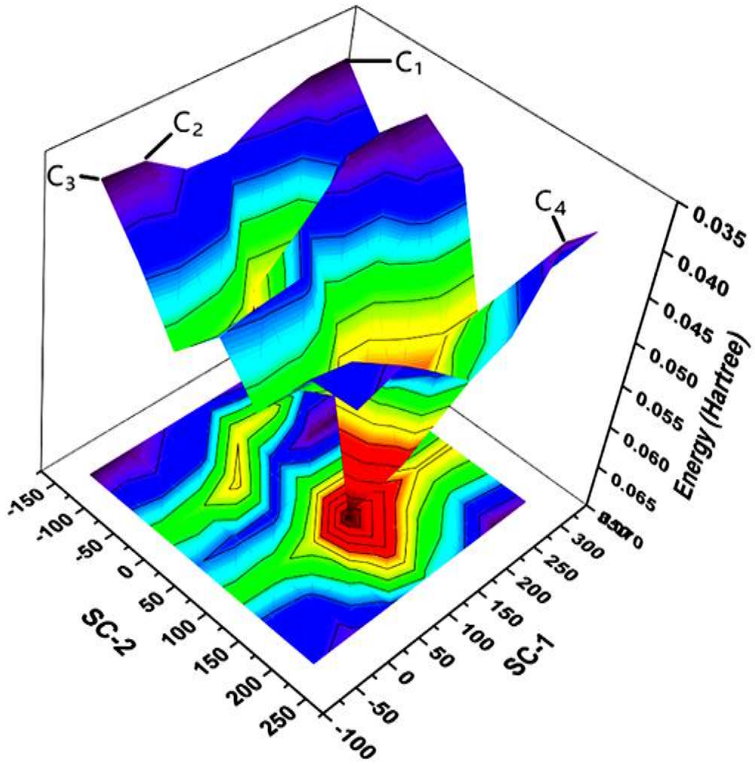

Investigation on spectra (UV-Vis, vibrational, NMR, HRMS), electronic structure (DFT calculations), molecular docking and antidiabetic activity of N-((benzo[*d*]thiazol-2-ylthio)methyl)-N-cyclohexylcyclohexanamine – A Mannich base

Krishnan Sarojini Devi [a], Palaniappan Subramani [b,] *, Namadevan Sundaraganesan [c], Maria Susai Boobalan [d], Dhanapal Tamilvendan [e]

[a] *Department of Chemistry, Sri-La-Sri Kasivasi Sawaminatha Swamigal Arts College, Thiruppanathal, Kumbakonam 612504, Tamil Nadu, India*

[b] *Chemistry Section, Faculty of Engineering and Technology, Annamalai University, Annamalainagar 608 002, Tamil Nadu, India*

[c] *Physics Section, Faculty of Engineering and Technology, Annamalai University, Annamalainagar 608 002, Tamil Nadu, India*

[d] *Department of Chemistry, College of Natural and Computational Sciences (CNCS), Haramaya University, Dire Dawa, Ethiopia*

[e] *Department of Chemistry, National Institute of Technology, Tiruchirappalli 620 015, Tamil Nadu, India*

*Corresponding author
Dr. P. Subramani
Professor
Chemistry Section
Faculty of Engineering and Technology
Annamalai University
Annamalainagar 608 002.
Tel.: +91 8973522231
E-mail: saro87che@gmail.com

ABSTRACT

A new Mannich base molecule of N-((benzo[*d*]thiazol-2-ylthio)methyl)-N-cyclohexylcyclohexanamine (ICF) has been synthesized and spectroscopic characterization such as FT-IR, FT-Raman, UV-Vis, NMR, mass and TG/DSC were investigated. The spectroscopic quantum chemical calculations namely simulation of vibrational spectrum, UV-Vis, NMR have been carried out and compared with the experimental observations. Other theoretical predictions such as Equilibrium Geometry, chemical reactivity, molecular electrostatic potential, frontier molecular orbital analysis and natural bond orbital analysis (NBO) have been computed and investigated using the density functional theoretical (DFT) methods. The computed entities and experimental results the consistently have good agreement with each other. The excited properties of ICF have been calculated using the TDDFT calculations. The molecular docking studies used to simulate the protein-ligand interactions have been analyzed with Schrödinger software.

Keywords: Mannich base, Density functional theory, Basis set, Mass, Natural bond orbital, Molecular docking

1. Introduction

A novel and a newly synthesized Mannich base molecule of N-((benzo[*d*]thiazol-2-ylthio)methyl)-N-cyclohexylcyclohexanamine (ICF), $C_{20}H_{28}N_2S_2$ has been synthesized by employing condensation of three reactants secondary amine, formaldehyde and active hydrogen compound. Generally, Mannich base compounds acting as a potential biological agents have been reported earlier. They play very significant applications such as analgesic drugs [1], vasorelaxing [2], anti-malarial [3], anti-tubercular [4] and anticancer [5]. The cyclohexylamine (CHA) can be used in the synthesis of artificial sweeteners (sodium or calcium cyclamate), metal corrosion inhibitors, rubber vulcanizing additives, dyestuff, plasticizers and in extracting agents for natural products [6]. The dicyclohexylamine is used industrially in chemical formulations as anti-corrosion agents (metal tools and spare parts). Dicyclohexylamine (DCH) is an excipient in commercial fumagillin formulations used in veterinary medicine. Nowadays, benzothiazoles have bicycles ring system of scientific interest for their various pharmaceutical applications which play vital role for the preparation of fused heterocyclic systems [7]. The heterocyclic thialato ligand of 2-mercaptobenzothiazole has potential N- and S-donors and synthesizes the complex prosperous in biological activities [8]. Benzothiazole and its derivatives widely display remarkably different bioactivities in the field of bioorganic and medicinal chemistry in drug discovery and in the agrochemicals field [9–12]. They are widely used in manufacture of rubber shoes, tyres, other related rubber articles and rubber vulcanization accelerator [13]. They are used as stabilizer and biocide commonly act as an inhibitor of copper corrosion within re-circulating of water systems [14]. Furthermore, the benzothiazole has significant interest as a collector of floating and is used for oxidizing the lead and copper minerals [15]. In the recent years, Lee et al. [16] analyzed the adsorption orientation of 2-mercaptobenzoxazole (MBO) and 2-mercaptobenzothiazole (MBT) with surface improved Raman scattering (SERS).

Author report, probably for the first time, the results based on quantum chemical calculations, FT-IR and FT-Raman spectral studies, HOMO-LUMO and NBO analysis on ICF molecule and also, for the first time it is reported that the synthesis procedure of ICF molecule using imide, aldehyde and secondary amine in acetonitrile medium. The ICF molecule is a yellow powder sample which has a melting point of 166 °C. The molecule ICF based on coarse aqueous suspension shows 7.98 pH having very less basicity level. Therefore the present work is mainly focused to investigate the complete vibrational spectra of the ICF molecule and to identify the different vibrational modes with better accuracy as well as the spectral characterization of the ICF molecule by quantum chemical method. Density functional theory (DFT) computations have been predicted to support the

vibrational frequencies in the FT-Raman and FT-IR spectra of the ICF molecule. Due to the diverse potential biological activity of the ICF molecule, the molecular docking of the ICF molecule has also been reported.

2. Experimental details

2.1. Synthesis of N-((benzo[d]thiazol-2-ylthio)methyl)-N-cyclohexylcyclohexanamine (ICF)

About 0.01 M of 2-mercaptobenzothiazole was dissolved in minimum quantity of ethanol and added steadily to saturated aqua solution of 0.01 M dicyclohexylamine with constant stirring. In addition to this mixture, about 0.01 M of formaldehyde was added gradually with continuous stirring. The mixture was stirred at room temperature for 2h and the progress of the reaction has been monitored by TLC. After 6 h, the greenish yellow colour solid product was obtained and washed several times with ethanol and water. It was then recrystallized with acetone. About 84% of the yield has been obtained. The melting point of the ICF molecule is 166 °C (Fig. 1).

2.2. Spectroscopy measurements

The FT-IR spectrum was carried out using the Perkin Elmer spectrophotometer with a resolution of 2 cm^{-1} and the scanning region from 4000–450 cm^{-1} besides having 100 numbers of scans by analyte the KBr pellet. The FT-Raman spectrum was obtained using the Bruker RFS 27: Stand-alone FT-Raman spectrometer by Nd:YAG laser source of wavelength 1064 nm with 1.0 cm^{-1} resolution in the span of 4000–50 cm^{-1} and 100 number of scans. The NMR spectra were conducted on a Bruker Avance spectrometer at 500 MHz for ^{1}H and ^{13}C NMR. The chemical shift values (δ) in the NMR spectrum were measured in parts per million (ppm) with comparative analysis to the reference sample as the TMS molecule. The mass spectrum was recorded using the Agilent 7890A GC system. Vario EL III Elementar was used to carry out the CHNS analysis. The UV-Vis spectrum was given by using Perkin Elmer Lambda 35 spectrometer between 250 to 700 nm. The TGA/DSC was recorded in TGA-50 Shimadzu-00652 instrument at a heating rate of 10 °C/min under atmospheric nitrogen.

2.3. Theoretical calculations

Theoretical calculations, evaluated with the Khon-Sham's DFT method, were subjected to the gradient-corrected hybrid density functional B3LYP method [17–19]. For the structure, the 6-31G(d, p) basis set was used for a full geometry optimization using the published function which was implemented by the Gaussian 09 package [20]. All the produced geometries were done by GaussView 5.0.9 [21] and/or Chemcraft 1.6 software packages [22]. The vibrational modes were assigned on the basis of PED analysis using VEDA4 program [23]. It should be noted that the Gaussian 09W package was able to calculate the Raman activity. The Raman activities were

transformed into Raman intensities using Raint program [24]. The ^{1}H and ^{13}C NMR chemical shifts of the ICF molecule have been obtained from the gauge-independent atomic orbital (GIAO) [25,26] approach by subtracting the shielding constants of TMS. The UV spectra were calculated using the TD-B3LYP-FC functional with 6-31G(d, p) basis set in methanol using TD-DFT model [27,28]. The DOS were computed by GaussSum 3.0 software [29]. The RDG calculation were made by Multiwfn [30] and VMD program [31]. The NBO calculation has been performed with NBO 3.1 program [32].

2.4. Raman intensities

The predicted Raman intensities (I_i^R) were determined by Raman activities (S_i) which were calculated using the Gaussian 09 package. Raman intensities can be described by the mathematical formula [33,34].

$$(I_i^R) = C(\nu_0 - \nu_i)^4 \nu_i^{-1} B_i^{-1} S_i \quad (1)$$

where the B_i is the temperature factor which interprets the intensity contribution of excited vibrational states, denoted by the Boltzmann appropriation.

$$B_i = 1 - (\exp - h\nu_i c/KT) \quad (2)$$

2.5. Docking studies

The molecular docking study was investigated by using the diabetic proteins to find the active binding sites and interaction properties of the amino acids with synthesized molecules. The 3D crystal structure of protein complex (PDB format) was downloaded from Protein Data Bank (www.rcsb.com). The protein complex and ligand were organized after pre-processing by protein preparation wizard and ligand preparation wizard [35] in Maestro 9.3.5 version of Schrödinger software.

2.6. In vivo antidiabetic assay

2.6.1. Animals and maintenance

Adult male albino Wistar rats (6 weeks), weighing 150 to 200 g were used for the present antidiabetic study. The animals were housed in clean polypropylene cages and maintained in a well-ventilated temperature controlled animal house with a constant 12 h light/dark schedule. The animals were fed with standard rat pelleted diet and clean drinking water was made available *ad libitum*. All the animal procedures were performed after approval from the ethical committee and in accordance with the recommendations for the proper care and use of laboratory animals.

2.6.2. Ethical statement

Antidiabetic procedures were carried out at Department of Pharmacology, KMCH College of Pharmacy, Coimbatore, with no anti-ethical statements.

2.6.3. Induction of diabetes

The animals were divided into five groups of six animals each. The animals were kept over night fasting and the initial fasting blood glucose was checked from the tip of rat-tail vein. Sterptozotocin (STZ) was dissolved in citrate buffer (pH 4.5) and nicotinamide (NA) was dissolved in normal saline. Non-insulin dependent diabetes mellitus was induced in overnight fasted rats by a single intraperitoneal (i.p) injection of 60 mg/kg STZ and 15 min after the i.p administration 120 mg/kg of NA was induced. After 72 h, the hyperglycemia was confirmed by the elevated levels of blood glucose. The animals with blood glucose concentration more than 250 mg/dL were used for the study [36].

2.6.3.1. Study design

After the acclimation for a period of one week, they were divided randomly among five groups consisting of six rats each. The following groups were maintained for a total period of 28 days.

Group 1 : Animals received normal pellet feed (Control)

Group 2 : Streptozotocin (STZ) (60 mg/kg bw) + nicotinamide (NA) (120 mg/kg bw)

Group 3 : STZ (60 mg/kg bw) + NA (120 mg/kg bw) rats treated with Metformin (MF) (10 mg/kg bw)

Group 4 : STZ (60 mg/kg bw) + NA (120 mg/kg bw) rats treated with ICF and TBF (10 mg/kg bw – low dose (L.D))

Group 5 : STZ (60 mg/kg bw) + NA (120 mg/kg bw) rats treated with ICF and TBF (20 mg/kg bw – high dose (H.D))

The vehicle (saline), standard Metformin (MF) and the test compounds were administered on the respective group animals for 28 days. Throughout the study period, the MF and test compounds were freshly dispersed in normal saline and distilled water before the administration. The fasting animal body, blood glucose level was estimated from tip of rat tail vein on 1^{st}, 7^{th}, 14^{th}, 21^{st} and 28^{th} day.

2.6.3.2. Estimation of blood glucose

Blood samples were collected from the tip of rat-tail vein and the glucose levels were estimated using a glucose oxidase-peroxidase reactive strips and a glucometer (Accu-Chek, Roche Diagnostics, USA).

2.6.3.3. Determination of body weight

The body weight of each animal in every group was additionally noted during the investigation duration.

2.7. Statistical analysis

All the tests of fasting blood glucose and body weight estimations were carried out in triplicates. The values expressed as the Mean±SD (n=3) were analyzed with one-way analysis of

variance (ANOVA) and the post hoc Dunnett's test. The difference between the groups were considered to be significant at $P<0.05$.

3. Result and discussion

3.1. Molecular geometry

The computed optimized parameters like bond lengths, bond angles, and dihedral angles given in Table 1 and compared with their related molecule data as given in literature [37,38]. The ICF molecule contains the electronegatively sulfur groups bonded with the carbon C_{11} atom of dicyclohexylamine amine moiety. The sulfur group (C–S) along with the benzothiazole moiety with termination is considered as an electron acceptor group. The ICF molecule consisting of one C=N bond, four C–S bonds, four C–N bonds, eighteen C–C bonds and twenty six C–H bonds is shown in Fig. 2. The bond distance of N_7=C_8 (1.297/1.285 Å) in the ICF molecule shows equivalent value for the normal value of double C=N (1.22 Å) and lower than the single bond value C–N (1.47 Å) as given in the literature [39]. The bond length of C_4–N_7 (1.389/1.340 Å) is greater than normal value of double C=N (1.22 Å) and lower than the single bond value C–N (1.47 Å) as given in the relevant literature [39]. Similarly, the bond length of N_{12}–C_{13} (1.485/1.506 Å) and N_{12}–C_{14} (1.477/1.506 Å) for dicyclohexylamine moiety are greater than normal value of double C=N (1.22 Å) and equivalent value for single bond C–N (1.47 Å) as given in the relevant literature [39]. Those values have resemblance with the 2-mercaptobenzothiazole due to the presence of resonance between –NH–C=S and –N=C–SH (thione-thiol tautomerism) reported earlier [40,41]. The bond lengths of C_5–S_9 for benzothiazole moiety 1.758/1.718 Å, C_8–S_9 (1.792/1.743 Å) and C_8–S_{10} (1.754/1.743 Å) are found intermediate compared to the single bond and double bond character, due to the attachment of neighbouring C=S group. In cyclohexyl ring, the C–C–C bond angle varies from 110.7–111.5°, so the cyclohexyl ring act as a chair configuration. The benzothiazole ring being essentially planar makes a bond angle around 120° with the dicyclohexylamine ring. The C–C bond length of benzothiazole ring with sp^2 character intermediate values are found between single and double bonds due to the presence of delocalization of electron within the ring C_1–C_2, C_1–C_6, C_2–C_3, C_3–C_4, C_4–C_5, C_5–C_6 such as 1.404, 1.394, 1.391, 1.401, 1.416 and 1.395 Å while those values are found concurrence with theoretical data 1.347, 1.366, 1.380, 1.415, 1.410 and 1.367 Å, respectively. In dicyclohexylamine ring, the bond length of C_{13}–C_{20} (1.544/1.519 Å), C_{13}–C_{24} (1.539/1.518 Å), C_{14}–C_{15} (1.540/1.519 Å), C_{14}–C_{19} (1.546/1.518 Å), C_{15}–C_{16} (1.537/1.525 Å), C_{16}–C_{17} (1.536/1.515 Å), C_{17}–C_{18} (1.535/1.512 Å), C_{18}–C_{19} (1.537/1.526 Å) are slightly deviated from the single bond properties due to the attachment of electronegative group nitrogen and oxygen atom. The C–H bond length of benzothiazole ring varies from 1.085–1.086 Å which is compared to the observed values (0.93

Å). In benzothiazole ring, the C–H bond distances are C_1–H_{25} (1.086/0.930 Å), C_2–H_{26} (1.086/0.930 Å), C_3–H_{27} (1.085/0.930 Å), C_6–H_{28} (1.085/0.930 Å). In dicyclohexylamine ring, the C–H bond length varies from 1.094–1.107 Å which is compared with the observed values 0.970–0.980 Å. In dicyclohexylamine ring, the C–H bond values are C_{13}–H_{31} (1.107/0.980 Å), C_{15}–H_{33} (1.097/0.970 Å), C_{15}–H_{34} (1.095/0.970 Å), C_{16}–H_{35} (1.099/0.970 Å), C_{16}–H_{36} (1.099/0.970 Å), C_{17}–H_{37} (1.099/0.970 Å), C_{17}–H_{38} (1.096/0.970 Å), C_{18}–H_{40} (1.098/0.970 Å), C_{19}–H_{41} (1.098/0.970 Å) and C_{19}–H_{42} (1.097/0.970 Å).

3.2. Potential energy surface (PES) scan

Due to the flexibility of N-((benzo[*d*]thiazol-2-ylthio)methyl)-N-cyclohexylcyclohexanamine and possible rotational isomerism, the potential energy surface (PES) scans about C_8–S_{10}–C_{11}–H_{29} (scan coordinate–1 (SC–1)) and H_{30}–C_{11}–N_{12}–C_{13} (scan coordinate–2 (SC–2)) were performed to confirm the theoretical approximation for the molecule. The torsion angle of C_8–S_{10}–C_{11}–H_{29} and H_{30}–C_{11}–N_{12}–C_{13} are found as the relevant coordinate for the conformation flexibility within the molecule. The PES calculation has been performed using PM3 semi-empirical method since the ab-initio and the DFT methods are costly for 10° interval scan with each step optimization. During the calculation all the geometrical parameters were simultaneously relaxed while the C_8–S_{10}–C_{11}–H_{29} and H_{30}–C_{11}–N_{12}–C_{13} torsion angles were found varying in steps of 0°, 10°, 20°, 30°, … 360°. For the SC–1 and SC–2 rotations, the maximum energy conformer has been appeared at 118.42 and 104.31 with 0.06964 Hartree energy on PES (Table 2). It's clearly mentioned in Fig. 3 with steep down apex red region. Around four different minimal energy conformers has been generated, namely C_1, C_2, C_3 and C_4 with 0.00007 Hartree energy difference. The conformers C_1, C_3 and C_2, C_4 have the same energy having different stereo chemical orientations. Although, the SC–1 and SC–2 of C_1, C_3 and C_2, C_4 are different, the energy is same. Interestingly, the ground state structure of ICF by DFT method simply reproduces the structure of C_1 conformer rather than the C_3 conformer with different dihedral value.

3.3. Vibrational analysis

There are 52 atoms present in the ICF molecule which exhibit 150 normal modes of vibrations with 52 stretching and 98 bending vibrations. The fundamental vibrational modes were calculated by using B3LYP/6-31G(d, p) basis set and compared with the experimental vibrational spectra. The entire spectral assignments with total energy distribution (TED) contributions are collected in Table 3. The experimental and theoretical FT-IR and FT-Raman spectra of the ICF molecule are shown in Figs. S1 and S2 for visual comparison. The vibrational modes of the functional groups in ICF molecule are described below:

3.3.1. C–S vibrations

Generally, it is difficult to identify the C–S stretching vibrational modes for various compounds in FT-IR spectrum. The absorption of C–S vibration has variable intensity which depends on the nature of the molecules which might be found with wide range 1035–245 cm^{-1} for aliphatic as well as aromatic [42]. The C–S group is less polar than the carbonyl group, so the peak appears in the weaker band in FT-IR. Since, the peak shows in lower frequencies, the less intense, coupling with other vibrational modes are not easily identified with this vibration. Xiao-Hong et al. [43] have reported, the C–S stretching vibrational mode was observed at 716–609 cm^{-1}. Similarly, the C–S stretching vibrational mode is observed at 690 cm^{-1} in the FT-IR spectrum and 691, 678, 495, 384 cm^{-1} in FT-Raman spectrum. The corresponding simulated values for C–S stretching vibrational mode were observed at 692, 679, 495 and 389 cm^{-1}.

3.3.2. C=N vibrations

Benzon et al. [44] have previously reported at 1463 cm^{-1} for simulated and observed value at 1463 cm^{-1} in FT-IR spectrum. In ICF molecule, the C=N stretching vibrational mode was observed at 1470 cm^{-1} in FT-IR and at 1469 cm^{-1} in FT-Raman spectrum. The simulated value was observed at 1470 cm^{-1} with corresponding TED contribution 72%. The in-plane vibration of –C=N, displayed at 630 cm^{-1} in FT-IR and at 629 cm^{-1} in FT-Raman was compared with the theoretical wavenumber at 631 cm^{-1} with a TED of 31%. The normal vibrational modes of a title molecule were overlapping with some bending vibration and C–C, C–S, C–H vibrations.

3.3.3. C–N vibrations

It is difficult to identify the C–N vibration due to mixing of several modes possible in this region. The C−N stretching vibrational mode was in the range from 1362–1266 cm^{-1} [45]. The assignment of C–N stretching vibrations of ICF molecule were observed at 1261, 1131 cm^{-1} in FT-IR and at 1263 cm^{-1} in FT-Raman spectrum. The correlated simulated spectrum was observed at 1263, 1132 cm^{-1} with corresponding TED contribution of 17, 24% respectively. The in-plane vibration of –C–N, displayed at 456 cm^{-1} in FT-IR and at 235 cm^{-1} in FT-Raman was compared with the theoretical wavenumber at 466, 240 cm^{-1} with a TED of ~15%. The vibration is exposed towards overlapping with some bending vibration and C–C, C–S, C–H vibrations.

3.3.4. C–C vibrations

In aromatic ring, the C=C, C–C stretching vibration modes are usually in the region 1650–1400 cm^{-1} [46,47]. In the present study, the C–C stretching vibration mode of benzothiazole ring fall in the frequency region of 1588 cm^{-1} in FT-IR spectrum and at 1560 cm^{-1} in FT-Raman spectrum. The corresponding C–C stretching vibration mode of theoretical counterpart appeared at 1593, 1561 cm^{-1} with TED contribution 60, 67%. Similarly, the C–C stretching vibration modes of dicyclohexylamine appeared at 1311, 1123, 1060, 1034, 756 cm^{-1} in FT-IR and at 1064, 1028, 986 cm^{-1} in FT-Raman

spectrum. The related theoretical counterpart of C–C stretching vibration modes of dicyclohexylamine were observed at 1315, 1128, 1065, 1061, 1035, 1028, 994, 756 cm^{-1}. The in-plane vibrations of C–C vibration were assigned at 1048, 443 cm^{-1} in FT-IR and 1042, 407 cm^{-1} in FT-Raman which were correlated value at 1050, 444, 408 cm^{-1} theoretically with contribution of ~35%. The out-plane vibration of C–C vibration was observed at 874 cm^{-1} in FT-Raman which are correlated at 877 cm^{-1} theoretically with contribution of 45%. The torsion vibration modes of C–C vibration appeared at 998, 834, 582, 567 cm^{-1} in FT-IR and 1000, 817, 506 cm^{-1} in FT-Raman which were concurrent with the theoretical counterparts at 1007, 840, 817, 582, 578, 514 cm^{-1} with the contribution of ~60%.

3.3.5. C–H vibrations

The C–H stretching vibration of aromatic ring exhibited the multiplicity of weak to moderate bands, when compared with the aliphatic C–H stretching vibration [48]. Klots and Collier [49] have previously reported about the vibrational modes at 3085, 3074, 3065 and 3045 cm^{-1} for benzoxazole. The C–H stretching vibrations of phenyl ring are observed in the 3120–3000 cm^{-1} Roeges [50]. In current study, the C–H stretching vibrations of benzothiazole ring are observed at 3055, 2999 cm^{-1} in FT-IR and at 3074, 2998 cm^{-1} in FT-Raman spectrum. The corresponding C–H stretching vibrations of benzothiazole ring for simulated spectrum appear at 3081, 3055 and 2999 cm^{-1} with TED contributions of above 75%. Commonly, the coordinate investigation exhibits that the aromatic C–H bending vibrational modes as overlapped with some stretching, in-plane and out-of-plane vibration mode (Table 3).

3.3.6. CH_2 vibrations

Generally, the C–H stretching vibrations appear in the region 2980–2900 cm^{-1} in FT-IR for aliphatic amine molecule [51]. In present study, the vibrational band appears at 2970, 2818 cm^{-1} in FT-Raman and in FT-IR at 2959, 2924, 2817 cm^{-1} is due to assignment of C–H stretching vibration for dicyclohexylamine. The related simulated wavenumber is coherent to the experimental and the reported data at 2971, 2965, 2927, 2819 cm^{-1} (with greater than 75% TED) by employing the B3LYP/6-31G(d, p) method. The fundamental vibrations of CH_2 owing to twisting, rocking, wagging, and scissoring are observed in the range from 1500–800 cm^{-1} and the bands show deviation in these wavenumbers owing to the presence of atom in nature and substituent of molecule linked to CH_2 group [52]. For dicyclohexylamine, the in-plane bending vibrations are assigned at 1450, 1311, 1241 cm^{-1} in FT-IR while the related simulating frequencies are found at 1456, 1315, 1244 cm^{-1} with pure vibration mode of TED greater than 70% [53]. The most vital point is that certain CH_2 modes are generally coupled with some stretching and bending vibrations (Table 3).

3.4. NMR spectral analysis

The molecular geometry of ICF molecule is optimized by DFT method with B3LYP/6-31G(d, p) basis level. The chemical shifts of ^{1}H and ^{13}C NMR have been carried out with the help of gauge invariant atomic orbital (GIAO) calculations. The experimental and simulated chemical shifts of ICF molecule in ^{1}H and ^{13}C chemical shifts values are noted in Table 4 and NMR spectra are exhibited in Fig. 4. The values show good agreement with the computed and experimented ^{1}H and ^{13}C chemical shifts.

3.4.1. ^{1}H NMR

The ^{1}H NMR chemical shift value of N–CH_2–S appears at 3.36 ppm deshielded region (high chemical shift value) indicating the presence of electronegative atom like Sulfur and Nitrogen atom. A multiplet peak was displayed in the deshielded region of 3.11–3.10 ppm with two protons (H_{31} and H_{32}), which were assigned to the cyclohexane ring protons due to the attachment of electron withdrawing group nitrogen atom. Another multiplet peak is assigned to eight equivalent aliphatic protons at 1.80–1.78 ppm (H_{33}, H_{34}, H_{41}, H_{42}, H_{43}, H_{44}, H_{51}, H_{52}) with eight protons of cyclohexane ring. Similarly, yet another multiplet peak was displayed at 1.90–1.88 ppm, which assigned to eight equivalent aliphatic hydrogens (H_{35}, H_{36}, H_{39}, H_{40}, H_{45}, H_{46}, H_{49}, H_{50}) of cyclohexane ring. The next multiplet peak was assigned as four equivalent aliphatic protons of cyclohexane ring at 1.77–1.66 ppm (H_{37}, H_{38}, H_{47}, H_{48}). The two set triplet peaks were presented at 7.16 (H_{25}) and 7.27 (H_{26}) ppm with integral value corresponding to the two aromatic protons having the coupling constant 6.4 and 6.6 Hz. A two set of doublet peaks were shown at 7.57 (H_{27}, J = 7.1 Hz) and 7.46 (H_{28}, J = 7.2 Hz) for aromatic protons in benzothiazole ring. The calculated values of proton chemical shifts were summarized in Table 4.

3.4.2. ^{13}C NMR

Generally, the ^{13}C NMR spectrum of aromatic compounds appear in the typical the region >100 ppm [54,55]. In the ^{13}C NMR spectrum of ICF molecule, the peak at 188.3 ppm (high chemical shift value) was assigned to the C_8 linked with electronegative sulfur atom and nitrogen atoms. Similarly, the signal at 148.3 ppm was assigned to be C_4 connected with electron withdrawing nitrogen atom. The chemical shift value of C_5 has a higher value, which happens due to bonding with the electronegative nitrogen atom, appeared deshielded region at 136.9 ppm. The three aromatic carbons were displayed at 121.0–126.4 ppm in carbon NMR spectrum. The signal at 121.0 ppm is assigned as C_3 position in benzothiazole ring. Another aromatic carbon C_2 of benzothiazole ring is exhibited at 126.4 ppm. The signal at 123.6 ppm was assigned as C_1 position in benzothiazole ring. The C_{13} and C_{14} were displayed at 64.8 ppm in the deshielded region due to the attachment of electronegative group nitrogen atom. The carbon C_{11} appears at 54.4 ppm, which had high chemical shift value (deshielded region) due to the attachment neighbouring electron withdrawing of sulfur and

nitrogen. The chemical shifts of cyclohexane ring are observed in the range from 25.7–31.2 ppm. The simulated and observed NMR results showed some deviations, because the computed calculation was done in gas phase and experimental work takes place in solid.

3.5. Mass spectrum

The mass spectrum of ICF molecule was obtained on HRMS. The mass spectrum of the ICF molecule is shown in Fig. 5a. The Fig. 4a illustrates the molecular ion peak at m/z = 399.1304 which confirms the molecular mass of the ICF molecule with K ion ($C_{20}H_{28}N_2S_2$), when compared with the calculated mass m/z = 399.1331.The peak appearing at m/z = 400.1304 corresponds to the protonated peak (M+1), $C_{20}H_{29}N_2S_2$. The ^{13}C, ^{15}N, and ^{33}S mainly contribute to the M+1 peak, of which the ^{13}C is found the most significant. If the M has the range up to 100%, the M+1 intensity/1.1% will give an approximation for the quantity of carbon atom present in the molecule.

3.6. TG/DSC analysis

The thermal characters of the solid ICF molecule were carried out by recording TG-DSC curve in the temperature which varied from 0 to 550 °C using the NETZSCH STA 449 F3 thermal analyzer under the nitrogen atmosphere and the heating was carried out at a rate of 20 °C/min. Fig. 5b indicates that the thermal decomposition of ICF molecule occuring in three consecutive steps. The initial step in TG curve illustrated the weight loss of 50.73% in the temperature range of 171.4–284.0 °C due to the exclusion of the methanethiol and hydrogen molecule groups from the title molecule, the second step showed the weight loss of 45.51% in the temperature range of 284.0–360.0 °C due to the decomposition of the ethanamine molecule from the former ICF molecule, the third step showed the mass loss of 99.13% in the temperature range of 360.0–516.5 °C due to the liberation of $C_6H_{13}N$ (cyclohexanamine) group and the complete decomposition of the molecule was finished. The nature of mass loss shows that there was neither volatilization nor fragmentation. A result of TG plot shows that the ICF molecule was stable up to 171.4 °C, when the fusion process beginning, followed by evaporation and no phase transition occurs till the melting point of the sample. The sample was defined as the unreality of crystallization from solvent or impurity and the most specific thermal steadiness of ICF up to beginning of melting point. The smooth response of the TGA curve behind its melting point represented the thermal liberation of ICF with the creation of reaction products [56]. The last residual carbon mass at 516.5 °C indicated the last part of the decomposition reaction is 0.87%. The second broad exothermic curve was shown at 273.1 °C and after this step the weight loss in TGA plot occured progressively. The progress weight loss illustrated the elimination of stable cyclohexanamine fragments [57].

The thermal decomposition temperature established as 284.0 °C in TGA graph, behind its melting point, indicates the thermal stability of the ICF molecule. There was no mass loss around 284.0 °C which represents the state at which no crystallization of phase transmission was possible. The DSC peak illustrates how the sample undergoes an irreversible exothermic transition where onsets of melting point and the peaks appeared at 168.2 and 273.1 °C. The initial exothermic weak peak appeared at 168.2 °C might be the melting point of the ICF molecule. The next exothermic peak appeared at 273.1 °C happens due to the decomposition of ethanamine. The definition of purity was based on the postulation that the contamination samples lower the melting point of a pure material. The melting point of a pure, high degree (100%) crystalline material have sharpness, but the impure sample or defects in the crystal structure will widen the melting point range and lower the melting point [58]. The material seemed to be appropriate for transparency determination by the DSC analysis; the material was established to be very pure (99.13%). The purity of the sample was confirmed by the obtained DSC result, less impurity content and also showed the acceptable results for the melting transition of the used material under various methods.

3.7. UV-Visible spectral analysis

The UV-Vis spectral analysis was carried out to explain the electronic transition within the molecule. In this study, to find out the maximum wavelengths, energy gap, oscillator strength and excitation energies of the ICF molecule which were obtained from B3LYP/6-31G(d, p) method. The observed UV-Vis spectra of the ICF molecule were carried out in chloroform as a solvent and computational calculations were used in gas and solvent phase as shown in Figs. S3 and S4. The broad peak and the maximum intensity of the title molecule clearly show that the charge transfer of interaction involved in the molecule. The molecular geometry calculation shows the maximum absorption wavelength of the ICF molecule which resembles the electron excitation from the top level of the occupied molecular orbital (HOMO) to lowest level of unoccupied orbital (LUMO).

The experimental value and computed value of UV-Visible spectral results were compared in Table 5. The predicted maximum excitation wavelength at 282 nm (f = 0.0069) in gas phase and 292 nm (f = 0.0047) were compared with the measured value at 326 nm (blue shift), it is represented as H-1→L (98%) electronic transition. The calculated and observed values show deviation and expected tolerance limit 34 nm. The experimental values mostly depend on the solvent effect. Therefore, the ICF molecule indicates the influence of solvent in optical activity as present in the molecule. The HOMO-LUMO electronic transformation occurs from the highest level of occupied molecular orbital at 97 level of molecular orbital number to lowest level of unoccupied orbital at 98 level, this occurs due to possible electronic transition in ICF molecule. In ICF molecule under chloroform condition, it

is observed that the initial peak from the n–π* electronic excitation due to electron transfer from dicyclohexylamine ring to benzothiazole ring. This is evidence for the n–π* electronic transition involved in the dicyclohexylamine ring where n determines the highest filled orbital while π* demonstrates the lowest unfilled level. The other two calculated values are 271, 261 with oscillator strength of 0.3548, 0.0722 in gas phase and 274, 261 nm with oscillator strength 0.5154, 0.0972 in solution phase respectively. These assignments correspond to the H-1→L (86%), H-2→L (6%), H-2→L (2%), H→L+2 (2%) and H-2→L (53%), H-1→L+1 (36%), H-1→L (7%) electronic transition. There is no peak of absorption in the entire visible region which evidently tells about its applicability towards frequency doubling process. The absorption of maximum of λ_{max} is the utility of substitution; the more electrons pushed into the ring, shows the higher value of λ_{max}.

3.8. Frontier molecular orbital analysis

The most important part of FMO was helpful in defining the chemical hardness-softness, optical polarizability and the chemical reactivity of the particular molecule. To define the various reaction types, the calculating reaction position in π-conjugated systems, MO and related their properties like energy are commonly used. The molecule having low energy gap has more polarizable property, which was associated with high chemical reactivity and low kinetic stability. These properties facilitate the chemists and physicists to know about the main role taking place in the chemical reaction. The energy of the HOMO is related to ionization potential and the LUMO is related to electron affinity of the molecule. Nowadays, the energy of HOMO, LUMO and their energy gap resolve the biological activity of the molecule from ICT [59,60].

In presence of conjugated molecules, the highest filled and lowest unfilled molecular orbital are characterized by charge separation of HOMO-LUMO as a result of the important role of intermolecular charge transfer (ICT) from end-capping electron of donor groups via π-conjugated way. The strong ICT that originates on the π-conjugated bridge results as a substantial ground state mixing of electron donor-acceptor groups, the charge transfer band appear in the absorption spectrum. As a result of FMO, the ED transfer from aromatic part of the π-conjugated system that act as an electron donor side to electron accepting part of MO. As a result of DFT calculations, the total number of molecular orbital consists of 410 FMOs and 98 occupied MOs and 312 unoccupied orbitals. The HOMO is mainly located on benzothiazole ring, dicyclohexylamine ring and the LUMO is mainly located on the same ring except sulfur (S_{10}), N_{12} and dicyclohexylamine ring. In experimental work, the common formula; $E = hc/\lambda$ is used to calculate the energy gap value. Here h and c are constant, λ is the cut-off wavelength. By ploting the hν against $(\alpha h\nu)^2$ to obtain an observed energy gap at 3.14 eV and compared with 4.41 eV (gas phase) and 4.24 eV (solvent phase) which are shown in

Table 6 and Fig. 6. The energy values of HOMO and LUMO in DOS spectrum are used to predict the global chemical reactivity description of the ICF molecule as shown in Table 7 and Fig. 7a. The energy values of HOMO, LUMO and the energy gap are –5.69, –0.68 and 5.01 eV in gas phase and 5.72, 0.85 and 4.87 eV in solvent phase, respectively. The higher ionization potential implies the high reactivity of a molecule. The hardness and softness are used to explain the stability and reactivity of a molecule. A large energy gap defined as hard molecule and low value indicates soft molecule [61]. In ICF molecule, the value of chemical hardness is higher than the softness, so the title molecule becomes more kinetically stable and less reactive as shown in Table 7. The electronegativity of a molecule is used to define the electrons attraction of an atom in a covalent bond. When two dissimilar atoms are covalently bonded, the sharing of electron will be more strongly attracted with each other, so the electronegativity becomes greater. The electrophilicity index was helpful to explain the lowering of energy based on the maximum number of electron transfer from HOMO to LUMO. As shown in Table 7, the ICF molecule had higher value which implied the strong electron excitation between HOMO and LUMO [62]. The electronic absorption mainly was explained by the electron excitation from the HOMO to LUMO which increased the stability of a molecule and decrease the ICT that makes the molecule as NLO active.

3.9. Total, partial and overlap population density of states

The vital role of DOS spectrum is used to describe the molecular orbital compositions and their percentage of contribution to chemical bonding *via* OPDOS peaks based on the COOP diagram in the literature. The PDOS spectrum explains the fragment orbital composition of atoms or groups which involve in the molecular orbital. The total, partial and overlapped populations in the density of states, defined as TDOS, PDOS and OPDOS spectrum can be got from GaussSum software by convoluting the molecular orbital information with Gaussian curves of unit height and full width at half maximum (FWHM) of 0.3 eV. The DOS, OPDOS and PDOS spectra are shown in Fig. 7. The OPDOS or COOP spectrum results, by multiplying of the DOS by overlapping population, are similar of DOS spectrum. The OPDOS spectrum displays the bonding, antibonding, non-bonding interaction between two atoms groups, orbitals. The positive value of COOP represented as the interaction of atoms or groups involves in bonding orbital and the negative value described as interaction of atoms or groups involves in antibonding orbital, zero value defined as interaction of atoms or groups involves in non-bonding orbital [63]. Both HOMO and LUMO are in FMO; they play vital role in chemical reaction of a molecule. The HOMO-LUMO energy gap is used to determine the electron transfer properties, so it is useful to calculate the electrical conductivity property of a title molecule [64]. The OPDOS is based on the Mulliken population with the help of GaussSum software. As a result of PDOS spectrum, the ICF molecule can be fragmented into four groups which are assigned

as nitrogen, sulfur, carbon and hydrogen as shown in Fig. 6c. The highest contribution comes from the nitrogen and sulfur and the least contributions come from carbon and hydrogen. Thus, the HOMO orbitals (H, C, S and N) are represented as (15% + 83% + 0% + 1% = 100%) whereas LUMO (H, C, O and N) are represented as (1% + 75% + 15% + 9% = 100%). However, the percentage contribution of atomic or molecular orbitals in the molecule is very hard to establish the bonding and antibonding character. So, the OPDOS diagram can be used as some of its orbitals of energy data results of interaction among the selected groups which are obtained from figure easily to identify the particular group of interactions as shown in Fig. 7b. In OPDOS spectrum, six groups were selected such as H overlap with C, H overlap with S, H overlap with N, C overlap with S, C overlap with N and S overlap with N.

3.10. Reduced density gradient (RDG) analysis

The weak interaction in real space of a molecule based on the electron density and their derivatives is described by Johnson et al. [65]. The RDG is a dimensionless quantity coming from the electron density with its first derivative. The weak interaction is defined as a position having electron density with low RDG value. The density value appears on the low-gradient spikes (the plot of RDG against ρ) which is explained as the strength of interaction of a molecule. The value of sign λ_2 is used to fully distinguish between bonding ($\lambda_2<0$) and non-bonding interaction ($\lambda_2>0$). The plot of RDG against electron density of ρ value multiplied by the sign of λ_2 can allow displaying the several interaction types present in the molecule. The RDG results are predicted by using Multiwfn and graphed by VMD program. The large positive value shows strong electron repulsion like steric effect and large negative value explains the strong non-covalent interaction for hydrogen bonding. Even either small positive or negative value describes the van der Waals interactions within a molecule. As a result of RDG, one or more spikes are present in low-density, low-gradient place as shown in Fig. 8a. The presence of weak interaction that implies to generated RDG isosurfaces which cover the related position in the real molecular space are shown in Fig. 8b.

3.11. NBO analysis

The results of the NBO analysis based on the second order perturbation are summarized in Tables S1 and S2. In the present study, the NBO analysis of ICF molecule shows six types of transitions such as strong σ–σ*, n–σ*, n–π*, π–π*, π–σ*, π*–π*, the hyperconjugative intra-molecular interactions produced by orbital interaction between bonding C–C, C–N, C=N, C=C, C–S and antibondings C–S, C–C, C–N, C=N, C=C and the bonding of lone pair atoms like N, S, with C–N, N=C, C–S and C=C antibonding orbitals contact with antibonding orbitals C=N, C=C which provide an intra-molecular electron density delocalization and creates the stability of a system.

As seen from Table S1, the highest stabilization energy value of ICF molecule for antibonding orbital shows antibonding (π orbital) C_4–C_5 to antibonding (π orbital) C_2–C_3 predicted at 180.61 kcal/mol (ED_i = 0.47592e) which implies the strong delocalized designate with the donor and acceptor groups. The other similar transitions are antibonding (π orbital) C_4–C_5 to antibonding (π orbital) C_2–C_3 and antibonding (π orbital) N_7–C_8 to antibonding (π orbital) C_4–C_5 and the related ED_i values are found as 0.47592, 0.38722e and stabilization energies are 153.99, 85.23 kcal/mol, respectively.

In lone pair, the highest stabilization energy value of ICF molecule shows LP(2)S_{10}→π*(N_7–C_8), LP(2)S_9→π*(N_7–C_8), LP(2)S_9→π*(C_4–C_5), LP(1)N_7→σ*(C_8–S_9), LP(1)N_{12}→σ*(S_{10}–C_{11}) and the related ED_i values are 1.80826, 1.70798 (2 and 3 are equal value), 1.87934 1.83606e and stabilization energy at 29.00, 24.67, 17.35, 17.25, 13.26 kcal/mol. In bonding (π) orbital, the highest stabilization energy value of ICF molecule shows π(C_2–C_3)→π*(C_4–C_5), π(C_4–C_5)→π*(C_1–C_6), π(C_2–C_3)→π*(C_1–C_6) and the related ED_i values are 1.69909, 1.63254, 1.69909e and stabilization energy at 21.03, 19.67, 19.58 kcal/mol. In bonding (σ) orbital, the highest stabilization energy value of ICF molecule shows σ(C_4–N_7)→σ*(S_8–C_{10}), and the related ED_i value is 1.97376e with the stabilization energy at 6.24 kcal/mol. The NBO analysis is used to define the hybridization of a title molecule as shown in Table S2. Table S2 shows the orbital type i.e., bond like (single or double) and the occupancy number of electrons range from 0.00 to 2.000. The types of orbital get bonded with lone pair of electron and antibonding orbital. The antibonding orbital is termed as non-Lewis structure. The ICF molecule shows some deviation due to the presence of electronegative atom like sulfur and nitrogen. The results of Table S2 show the bond of C_4–N_7 has electron density 1.97376 with 28.99% C_4 character in $sp^{2.45}$ and 70.95% N_7 character in $sp^{2.05}$ hybrid. The $sp^{2.45}$ hybrid on carbon (C_4) has 28.99% of p-character and $sp^{2.05}$ hybrid has 70.95% on nitrogen (N) p-character. It is efficient to identify sp^3 has 70% p-character as referred from given literature [66].

ICF molecule consisting of electronegative atoms sulfur and nitrogen get the higher value of polarization coefficients and also the atom connected with electronegative atom (sulfur and nitrogen) give low value of polarization coefficients. The percentage compositions of a title molecule are obtained from square of the polarization coefficient value involving in the natural bonding. From the NBO results, I have predicted the subsequent bonds such as C_4–N_7, C_5–S_9, N_7–C_8, N_7–S_9, C_7–N_{37}, C_8–S_{10}, S_{10}–C_{11}, C_{11}–N_{12}, N_{12}–C_{13} and N_{12}–C_{14}. The σ bond character of C_4–N_7 is composed of 0.6417C($sp^{2.45}$) + 0.7669N($sp^{2.05}$). The numbers 0.6417C + 0.7669N describe the polarization coefficient. The higher value of polarization coefficient indicates the higher electron density (%) of the NBO and also the increasing the electronegativity character of the atom [67]. The

weights are given from the squares of the polarization coefficient as $(0.6417)^2$ = 0.2899, corresponding to 28.99% localization on carbon atom. In an analogous method, the 70.95% on nitrogen atom is obtained. The NBO method was more polarized towards nitrogen atom, indicating the electronegative properties of nitrogen as noted in atomic charge analysis. The other bonds are explained in Table S2 along with polarization coefficient and their hybridization. The theoretical calculations were prepared by the available literature [68,69].

The natural hybrid orbitals with lower energies and high occupation numbers are: $n_1(S_{10})$, $n_1(S_9)$, $\sigma(N_7–C_8)$, $\sigma(C_2–C_3)$, $\sigma(C_1–C_2)$ and $\sigma(C_4–C_5)$. The corresponding energy values such as –0.24566, –0.65418, –0.88404, –0.68687, –0.68038, –0.69310 a.u, the considerable p-characters 31.38, 33.45, 61.99, 64.21, 64.71, 66.38%, the lower occupation numbers 1.98230, 1.98424, 1.98949, 1.97873, 1.98090, 1.97422 and the higher energy values with lower occupation number are $\pi(C_4–C_5)$, $\pi(C_2–C_3)$, $\pi(C_1–C_6)$, $n_1(S_{10})$ and $\pi(N_7–C_8)$. The corresponding energies are –0.69310, –0.68687, –0.24434, –0.62975, –0.32600 and considerable p-character 99.97, 99.96, 99.94, 99.92% and occupation numbers are 1.63254, 1.69909, 1.69582, 1.80826, 1.90265. Thus, a very near to pure p-type lone pair orbital participates in the electron donation to the $n_2(S_9)\rightarrow\pi^*(C_4–C_5)$, $n_2(S_9)\rightarrow\pi^*(N_7–C_8)$, $n_2(S_{10})\rightarrow\pi^*(N_7–C_8)$, $\pi(C_1–C_6)\rightarrow\pi^*(C_2–C_3)$, $\pi(C_1–C_6)\rightarrow\pi^*(C_4–C_5)$, $\pi(C_2–C_3)\rightarrow\pi^*(C_1–C_6)$, $\pi(C_2–C_3)\rightarrow\pi^*(C_4–C_5)$, $\pi(C_4–C_5)\rightarrow\pi^*(C_1–C_6)$, $\pi(C_4–C_5)\rightarrow\pi^*(C_2–C_3)$, $\pi(C_4–C_5)\rightarrow\pi^*(N_7–C_8)$, $\pi(N_7–C_8)\rightarrow\pi^*(C_4–C_5)$ interactions in the molecule.

3.12. Mulliken population analysis

The Mulliken population atomic charges have an enormous role in the field of DFT studies based on quantum chemical calculation through the entire molecular structure. The simulated Mulliken charge for the ICF molecule by B3LYP compared with the compositional groups such as N-methylbenzothiazole and N-methyldicyclohexylamine summarized in Table S3. The horizontal bar diagram of comparative Mulliken atomic charges are shown in Fig. S5. The comparison of the Mulliken atomic charge distribution in the ICF molecule and its individual N-methylbenzothiazole moiety represent the Mulliken atomic charge distribution as nearly equal in the aromatic ring and the carbon C_5, C_8, C_{11} having greater negative charge value; but the C_5 undergoes more opposite charge for ICF molecule than the separated N-methylbenzothiazole molecule. The Mulliken charge analysis of S_9 and S_{10} in ICF molecule has greater positive value than N-methylbenzothiazole molecule. This concludes the attachment of the N-methylbenzothiazole ring in the ICF molecule. Similarly, the N-methyldicyclohexylamine ring in the ICF molecule shows deviation of Mulliken atomic charges from that of the individual N-methyldicyclohexylamine in the carbon atoms like C_{13} and C_{14} *i.e.*, +I indicative effect. This is due to attachment of N-methylbenzothiazole moiety in the ICF molecule.

The highest negative value is observed at carbon (C_1) atom and this occurs due to the dislocation of electron, sulfur atom. The highest positive value is observed at C_4 carbon atom. This is influence the attachment of neighbouring nitrogen atom. Almost the entire hydrogen atoms exhibit positive charge and the maximum of carbon, sulfur, nitrogen atoms possess the negative charge. As a result of the electronegative character atoms, I have recognized the atoms which can take place electrophilic substitution at these centers.

3.13. Fukui function

The concept of generalized philicity [70] contains almost all the information about the known different global and local reactivity and selectivity descriptor, in addition to the information regarding electrophilic/nucleophilic power of a given atomic site in a molecule. Under this situation, the reactivity descriptor Δf(r) provides useful information on both stabilizing and destabilizing interactions between a nucleophile and an electrophile, which helps in identifying the electrophilic/nucleophilic behaviour of a specific site within a molecule. It provides positive value (positive value i.e., $\Delta f(r)>0$) for site prone for nucleophilic attack and a negative value (negative value i.e., $\Delta f(r)<0$) prone for electrophilic attack and these values are summarized in Table S4.

From the Fig. 9, the purple or bluish colour indicates the positive colour, i.e., the areas represent as a function positive, while red colour indicates the negative colour, i.e., the areas represents as a function negative. It can be seen from Fig. 9 that positive values of Fukui f_k^+ function of the title molecule are located at sulfur atom, which indicates the increase of electron density in this region, so the molecule acts as a nucleophilic attack. On the other side, the negative values of Fukui f_k^- functions are situated at the N–CH_2–N, which implies that the electron density losses, so the molecule acts as an electrophilic attack.

3.14. Local reactivity descriptors analysis

The local reactivity descriptors of a molecule based on the electron density are helpful to predict the probable reactive sites of the molecule, which are a significant for designing a medicinal compound. The softness (sf_k^+, sf_k^-, sf_k^0) and electrophilicity indices (ωf_k^+, ωf_k^-, ωf_k^0) were computed for the ICF molecule using Mulliken charge analysis to determine the possible electrophilic and nucleophilic reactive sites of atoms with in a molecule [71].

The values of local reactivity descriptors of a molecule for selected atomic reactive sites of using Mulliken charge distribution analyses are listed in Table S5. In ICF molecule, the highest values of the electrophilic reactivity descriptors (s_k^+, ω_k^+) at C_3 of benzothiazole ring moiety confirm that this is the most electrophilic site. Therefore, the C_3 is the most active site for nucleophilic attack and favour the formation of new heterocyclic compounds by an attack of nucleophilic part of the dipolar reagent. In the same way, the maximum values of the local nucleophilic reactivity descriptors (s_k^-,

ω_k^-) at N_{12} of cyclohexane ring moiety indicate that this is the most nucleophilic site. Therefore, this site is more prone to electrophilic attack and favours the formation of Schiff base. The C_4 position of benzothiazole ring is proved to be free radical attack.

3.15. Molecular electrostatic potential

The molecular electrostatic potential (MEP) is found very useful tool to reactive sites of a molecule related with electron density [72]. The MEP surface of the ICF molecule is mapped with colour code range from 0.3199 to –0.3199 a.u as shown in Fig. S6. The MEP image of ICF molecule displays two major negative potential regions around sulfur of benzothiazole (represented by red colour) and around the sulfur atom of methylene group (yellow colour) and the most positive potential located on nitrogen atom, cyclohexylamine ring and all hydrogen atom (blue colour). With the result of MEP diagram, they can infer that the H atom implying presence of strong attraction and sulfur implies the strong repulsion. The MEP mapped (vdW) surface is shown in Fig. S6b. It is used to describe the global maxima and minima of MEP on vdW surface. The contour plot of molecular electrostatic potential of ICF molecule has been made by the DFT method as shown in Fig. S6c. This conforms the positive and negative potential sites of a molecule according to the electron density surface.

3.16. Molecular docking studies

The molecular docking studies were used to resolve the binding reactive sites and the interactions among the synthesized molecule (ligand) and the protein. The target proteins are downloaded from the protein data bank. The ligand is prepared from the optimized molecular structure of the ICF molecule. The strength of the drug-receptor complex was successfully made by several features like hydrogen bond interactions, van der Waals forces, π–π stacking, hydrophilic and hydrophobic interactions. These interactions among the ligand and protein depend upon the nature of functional groups present in the ligand. The docking score of the ICF molecule with diabetic proteins 1Z32 and 3G7V are –5.56 and –5.53 as presented in Table S6. In 3D and 2D structure of docking results were clearly explained in the tested compound display of π–π stacking interactions of benzothiazole ring in ICF molecule with TRP 59 amino acids present in the active site of 1Z32 and 3G7V as shown in Fig. 10. The result of docking of ICF molecule shows the activity against the diabetic as compared to the experimental results.

3.17. In vivo antidiabetic activity

Organization of Streptozotocin (STZ) + Nicotinamide (NA) in animals speedily destroy the pancreatic β-cells, therefore, it provides approximately a decrease of discharge of insulin indicating

the type 2 diabetics [73] for insulin resistance. In our current study, it is found an increase in blood glucose level along with diabetic animals confirmed the installation of diabetic mellitus.

3.17.1. Analysis of blood glucose level

The effect of ICF on plasma glucose was exhibited in Table S7 and Fig. 11. The STZ (60 mg/kg bw) + NA (120 mg/kg bw) fed rats showed significant increase in the level of plasma glucose. Treatment with ICF decreased the levels of plasma glucose. With the two tested doses of ICF at a dose of 20 mg/kg show more significant decrease with plasma glucose level than the low dose.

3.17.2. Analysis of body weight

Table S8 and Fig. 12 show the changes in the levels of body weight in the control and experimental groups. At the end of the experimental period, the body weight was found significantly decreased in diabetic rats when compared to the normal rats (control), due to excessive catabolism of protein which provides amino acids for gluconeogenesis. Insulin deficiency resulted in muscle wasting decreases the body weight. The treatment with different doses of ICF (10 and 20 mg/kg bw) significantly increased the body weight among treated the diabetic rats.

4. Conclusion

DFT tools may useful to calculate the feasible activity spectrum of a reasonable drug molecule. The novel Mannich base ICF molecule was synthesized by using thiazole, aldehyde, amine and ethanol as a solvent. The synthesized molecule was characterized using various spectral techniques. The optimized molecular structure of the ICF molecule showed some deviation for bond lengths (C–S, C–N) and bond angles (C–C–C, C–C–N, H–C–C) due to the presence of benzothiazole and dicyclohexylamine moiety linked by methylene derivative (–N–CH_2–N–). Mulliken charge in the sulfur and carbon atom might contribute positively to show the biological activity of the ICF molecule. In UV-Vis spectrum, the λ_{max} corresponds to electron excitation from HOMO-LUMO with 98% contribution. The DOS spectrum and RDG diagram are also support for intramolecular interactions with in the molecule. The gradients of H, S and C_v increase with the increase of temperature owing to the enhancement of vibration of molecule. Almost all proposed and the synthesized ICF molecule has good docking score as diabetic proteins 1Z32 and 3G7V. These diabetic proteins can be confirmed as the most appropriate target protein through which the anticipated molecules, as well as planned prepared novel molecule show their diabetic activity. Virtual screening modelling best pharmacokinetics and ADME properties have positive potential bioactivity score against human receptors. The metabolic site likely to undergo metabolism were also performed. Docking results clearly shows ICF molecule (Hydrogen bonding, and Van der Waals interaction with ligand and target protein) to be an encouraging anti-diabetic agent and it might be referred as potential “lead molecule” for the synthesized of the novel anti-diabetic drug candidate.

Additionally, these data range predicted that title molecule has best oral bioavailability. The results obtained from this study may be valuable, which may be helpful to strategize out the further synthesis, in vivo testings which could lead to the appearance of novel inhibitors against diabetic activity. This study is helpful to report antidiabetic activity of novel ICF molecule. This synthesized ICF molecule showed better hypoglycemic activity. These results indicate that benzothiazole could be served as potential antidiabetic agents in the similar manner as thiazole derivatives. In diabetic activity, I have concluded that the administration of ICF dose dependently to STZ + NA induced type 2 diabetic rats ameliorated blood glucose and improved body weight. The overall quantum chemical spectral studies, electronic structure, various interactions and thermochemical property on antidiabetic active of ICF molecule were to extend the application in the field of medicinal and molecular modeling.

References

[1] W. Malinka, P. Swiatek, B. Filipek, J. Sapa, A. Jezierska, A. Koll. Synthesis, analgesic activity and computational study of new isothiazolopyridines of Mannich base type. Farmaco 60 (2005) 961–968.

[2] M.G. Ferlin, G. Chiarelotto, F. Antonucci, L. Caparotta, G. Froldi. Mannich bases of 3H-pyrrolo[3,2-f]quinoline having vasorelaxing activity.Eur. J. Med. Chem. 37 (2002) 427–434.

[3] F. Lopes, R. Capela, J.O. Goncaves, P.N. Horton, M.B. Hursthouse, J. Iley, C.M. Casimiro, J. Bom, R. Moreira, Tetrahedron Lett. 45 (2004) 7663–7666.

[4] S. Joshi, N. Khosla, P. Tiwari. In vitro study of some medicinally important Mannich bases derived from antitubercular agent. Bioorg. Med. Chem. 12 (2004) 571–576.

[5] B.S. Holla, B. Veerendra, M.K. Shivananda, B. Poojary. Synthesis characterization and anticancer activity studies on some Mannich bases derived from 1,2,4-triazoles**.** Eur. J. Med. Chem. 38 (2003) 759–767.

[6] S. Narayanan, R. Unnikrishnan, V. Vishwanathan. Nickel-alumina prepared by constant and varying pH method: Evaluation by hydrogen-oxygen chemisorption and aniline hydrogenation, Appl. Catal. A 129 (1995) 9–19.

[7] I. Caleta, D. Cincic, G. Karminski-Zamola, B. Kaitner, J. Chem. Crystallogr. 38 (2008) 775–780.

[8] E.S. Raper, Coord. Chem. Rev. 61 (1985) 115–184.

[9] D.A. Horton, G.T. Bourne, M.L. Smythe. The combinatorial synthesis of bicyclic privileged structures or privileged substructures. Chem. Rev. 103 (2003) 893–930.

[10] M.S. Chua, D.F. Shi, S. Wrigley, T.D. Bradshaw, I. Hutchinson, P.N. Shaw, D.A. Barrett, L.A. Stanley, M.F.G. Stevens. Antitumor Benzothiazoles. 7. Synthesis of 2-(4-Acylaminophenyl)benzothiazoles and Investigations into the Role of Acetylation in the Antitumor Activities of the Parent Amines. J. Med. Chem. 42 (1999) 381–392.

[11] P. Sharma, A. Mandloi, S. Pritmani. Synthesis of new 2-(substituted benzothiazolylcarbamoy l)benzimidazoles as potential eNS depressants. Indian J. Chem. 38B (1999) 1289–1294.

[12] M. Kawakami, K. Koya, T. Ukai, N. Tatsuta, A. Ikegawa, K. Ogawa, T. Shishido, L.B. Chen. Structure-activity of novel rhodacyanine dyes as antitumor agents. J. Med. Chem. 41 (1998) 130–142.

[13] H.P. Koch, Absorption spectra and structure of organic sulphur compounds. Part III. Vulcanisation accelerators and related compounds. J. Chem. Soc. (1949) 401–408.

[14] M. Ohsawa, W. Suetaka. Spectro-electrochemical studies of the corrosion inhibition of copper by mercaptobenzothiazole. Corros. Sci. 19 (1979) 709–722.

[15] G. Contini, A. Ciccioli, C. Cozza, M. Barbaro, A.M. Marabini. Infrared study of 2-mercaptobenzothiazole and two of its derivatives adsorbed on PbS. Int. J. Miner. Process. 51 (1997) 283–291.

[16] C.J. Lee, S.Y. Lee, M.R. Karim, M.S. Lee. Comparison of the adsorption orientation for 2-mercaptobenzothiazole and 2-mercaptobenzoxazole by SERS spectroscopy**.** Spectrochim. Acta A 68 (2007) 1313–1319.

[17] a) A.D. Becke, J. Chem. Phys. 98 (1993) 5648–5652; b) A.D. Becke, J. Chem. Phys. 96 (1992) 2155–2160.

[18] C. Lee, W. Yang, R.G. Parr. Development of the Colle-Salvetti correlation-energy formula into a functional of the electron density. Phys. Rev. B 37 (1988) 785–789.

[19] B. Miehlich, A. Savin, H. Stolt, H. Preuss. Results Obtained With The Correlation Energy Density Functionals Of Becke And Lee, Yang And Parr. Chem. Phys. Lett. 157 (1989) 200–206.

[20] M.J. Frisch, G.W. Trucks, H.B. Schlegel, G.E. Scuseria, M.A. Robb, J.R. Cheeseman, G. Scalmani, V. Barone, B. Mennucci, G.A. Petersson, H. Nakatsuji, M. Caricato, X. Li, H.P. Hratchian, A.F. Izmaylov, J. Bloino, G. Zheng, J.L. Sonnenberg, M. Hada, M. Ehara, K. Toyota, R. Fukuda, J. Hasegawa, M. Ishida, T. Nakajima, Y. Honda, O. Kitao, H. Nakai, T. Vreven, J.A. Montgomery Jr, J.E. Peralta, F. Ogliaro, M. Bearpark, J.J. Heyd, E. Brothers, K.N. Kudin, V.N. Staroverov, R. Kobayashi, J. Normand, K. Raghavachari, A. Rendell, J.C. Burant, S.S. Iyengar, J. Tomasi, M. Cossi, N. Rega, J.M. Millam, M. Klene, J.E. Knox, J.B. Cross, V. Bakken, C. Adamo, J. Jaramillo, R. Gomperts, R.E. Stratmann, O. Yazyev, A.J. Austin, R. Cammi, C. Pomelli, J.W. Ochterski, R.L. Martin, K. Morokuma, V.G. Zakrzewski, G.A. Voth, P. Salvador, J.J. Dannenberg, S. Dapprich, A.D. Daniels, O. Farkas, J.B. Foresman, J.V. Ortiz, J. Cioslowski, D.J. Fox, Gaussian 09, Revision A.02, Gaussian, Inc., Wallingford CT, 2009.

[21] R. Dennington, T. Keith, J. Millam, GaussView, Version 5.0.8, Semichem Inc., Shawnee Mission, KS, 2009.

[22] ChemCraft, Silicon/Manganese metal, SGS Audited Suppliers JH Silicon ISO9001:2015, http://www.chemcraftprog.com

[23] M.H. Jamroz, Vibrational Energy Distribution Analysis VEDA 4, Warsaw, 2004–2010.

[24] D. Michalska, RAINT, A computer program for calculation of Raman intensities from the Gaussian outputs, Wrocław University of Technology, 2002.

[25] M. Rohlfing, L.C. Allen, R. Ditchfield. Proton and carbon-13 chemical shifts: Comparison between theory and experiment. Chem. Phys. 87 (1984) 9–15.

[26] K. Wolinski, J.F. Hinton, P. Pulay, Efficient implementation of the gauge-independent atomic orbital method for NMR chemical shift calculations. J. Am. Chem. Soc. 112 (1990) 8251–8260.

[27] M.E. Casida, K.C. Casida, D.R. Salahub, Int J Quantum Chem. 70 (1998) 933–941.

[28] R.E. Stratmann, G.E. Scuseria, M.J. Frisch. An efficient implementation of time-dependent density-functional theory for the calculation of excitation energies of large molecules. J Chem Phys. 109 (1998) 8218–8224.

[29] N.M. O'Boyle, A.L. Tenderholt, K.M. Langner. cclib: A library for package-independent computational chemistry algorithms. J. Comput. Chem. 29 (2008) 839–845.

[30] T. Lu, F. Chen, Multiwfn: A multifunctional wavefunction analyzer. J. Comput. Chem. 33 (2012) 580–592.

[31] W. Humphrey, A. Dalke, K. Schulten. VMD: Visual Molecular Dynamics. J. Mol. Graph. 14 (1996) 33–38.

[32] E.D. Glendening, A.E. Reed, J.E. Carpenter, F. Weinhold, NBO Version 3.1, Theoretical Chemistry Institute, University of Wisconsin, Madison, WI, 1998.

[33] S. Shen, G.A. Guirgis, J.R. Durig. Spectra and Structure of Silicon-Containing Compounds. $XXVIII_1$ Infrared and Raman Spectra, Vibrational Assignment, and Ab Initio Calculations of Vibrational Spectrum and Structural Parameters of Vinyltrichlorosilane. Struct. Chem. 12 (2001) 33–43.

[34] D. Michalska, R. Wysokinski. The prediction of Raman spectra of platinum(II) anticancer drugs by density functional theory**.** Chem. Phys. Lett. 403 (2005) 211–217.

[35] Maestro, Version 9.3.5, Schrödinger, LLC, New York, 2014.

[36] M.A. Satheesh, L. Pari. Effect of pterostilbene on lipids and lipid profiles in streptozotocin–nicotinamide induced type 2 diabetes mellitus. J. Appl. Biomed. 6 (2008) 31–37.

[37] F. Al-Omran, A.A. El-khair, Studies and X-ray Determinations with 2-(Acetonylthio)benzothiazole: Synthesis of 2-(Benzothiazol-2-ylthio)-1-phenylethanone and

2-(Acetonylthio)Benzothiazole by C—S Bond Cleavage of 2-(Acetonylthio)benzothiazole in KOH. J. Heterocyclic Chem. 51 (2014) 62–70.

[38] D. Ndoye, M.M. Sow, L. Diop. Bis(dicyclohexylammonium) sulfate dihydrate. Acta Crystallogr. E 70 (2014) o237.

[39] S. Rajeswari, G. Venkatesa Prabhu, D. Tamilvendan, V. Ramkumar. Spectroscopic Studies and Crystal Structure of 1-(Morpholino (Phenyl) Methyl) Pyrrolidine-2,5-Dione. J. Chem. Crystallogr. 40 (2010) 437–442.

[40] J.P. Chesick, J. Donohue. The molecular and crystal structure of 2-mercaptobenzothiazole. Acta Crystallogr. B 27 (1971) 1441–1444.

[41] A. Tadjarodi, F. Adhami, Z. Gharehdaghi, G. Kickelbick. Synthesis and Crystal Structure of a Novel Mixed Ligand Cadmium(II) Complex of Benz-1,3-Thiazoline-2-Thione and 1,10-Phenanthroline. J. Chem. Crystallogr. 39 (2009) 368–371.

[42] C. Cirak, Y. Sert, F. Ucun. Effect of intermolecular hydrogen bonding, vibrational analysis and molecular structure of 4-chlorobenzothioamide. Spectrochim. Acta A 113 (2013) 130–136.

[43] L. Xiao-Hong, T. Zheng-Xin, Z. Xian-Zhou, Spectrochim. Acta A 74 (2009) 168–173.

[44] K.B. Benzon, H.T. Varghese, C.Y. Panicker, K. Pradhan, B.K. Tiwary, A.K. Nanda, C. Van Alsenoy. Spectroscopic and theoretical characterization of 2-(4-methoxyphenyl)-4,5-dimethyl-1H-imidazole 3-oxide. Spectrochim. Acta A 151 (2015) 965–979.

[45] F.R. Dollish, W.G. Fately, F.F. Bantley, Characteristics of Raman frequencies of organic compounds, John Wiley & Sons, Inc., New York, 1974.

[46] P.B. Nagabalasubramanian, S. Periandy, S. Mohan, M. Govindarajan. FTIR and FT Raman spectra, vibrational assignments, ab initio, DFT and normal coordinate analysis of alpha,alpha dichlorotoluene. Spectrochim. Acta A 73 (2009) 277–280

[47] Boobalan, M.s., Amaladasan, M., Ramalingam, S., Tamilvendan, D., Venkatesa Prabhu, G., Bououdina, M. First principles and DFT supported investigations on vibrational spectra and electronic structure of 2-((phenylamino)methyl)isoindoline-1,3-dione – An antioxidant active Mannich base. Spectrochimica Acta Part A: Molecular and Biomolecular Spectroscopy. 2015, 137, 962-78.

[48] J. Coates, Interpretation of infrared spectra, a practical approach, In: R.A. Meyers (Ed.), Encyclopedia of Analytical Chemistry, John Wiley & Sons Ltd, Chichester, 2000, pp. 10815–10837.

[49] T.D. Klots, W.B. Collier. Heteroatom derivatives of indene Part 3. Vibrational spectra of benzoxazole, benzofuran, and indole. Spectrochim. Acta A 51 (1995) 1291–1316.

[50] N.P.G. Roeges, A guide to complete interpretation of infrared spectra of organic structures, John Wiley & Sons, Chichester, New York, 1994.

[51] E. Gornicka, J.E. Rode, E.D. Raczynska, B. Dasiewicz and J.C. Dobrowolski, Vib. Spectrosc. 36 (2004) 105–115.

[52] M. Silverstein, G.C. Basseler, C. Morill, Spectrometric identification of organic compounds, 4th edn., John Wiley & Sons, New York, 1981, pp. 201–210.

[53] M. Suresh, M.S.A. Padusha, K. Govindarasu, E. Kavitha. Synthesis, structural and spectral analysis of 1-(pyrazin-2-yl) piperidin-2-ol by density functional theory. Spectrochim. Acta A 138 (2015) 271–282.

[54] H.O. Kalinowski, S. Berger, S. Brawn, Carbon-13 NMR Spectroscopy, John Wiley & Sons, Chichester, 1988.

[55] K. Pihlajer, E. Kleinprter (Eds.), Carbon-13 Chemical Shifts in Structure and Spectrochemical analysis, VCH Publishers, Deerfield Beach, 1994.

[56] T.J. Beaula, I.H. Joe, V.K. Rastogi, V.B. Jothy. Spectral investigations, DFT computations and molecular docking studies of the antimicrobial 5-nitroisatin dimer. Chem. Phys. Lett. 624 (2015) 93–101.

[57] R. Bottom, Chapter 3 - Thermogravimetric analysis. In: P. Gabbott (ed.), Principles and applications of thermal analysis, Blackwell Publishers, UK, 2008, pp. 88–118.

[58] T. Hatakeyama, Z. Liu, Handbook of thermal analysis, John Wiley & Sons, New York, 1998.

[59] C. Ravikumar, I.H. Joe, V.S. Jayakumar. Charge transfer interactions and nonlinear optical properties of push–pull chromophore benzaldehyde phenylhydrazone: A vibrational approach. Chem. Phys. Lett. 460 (2008) 552–558.

[60] Gajalakshmi, D., Boobalan, M.S., Vijay Solomon, R., Tamilmani, V. Are vinyl coupled furan derivatives better than vinyl coupled thiophene derivatives for optoelectronic applications? – Answers from DFT/TDDFT calculations. Computational Materials Science. 2019, 162, 60-8.

[61] Anandhan, K., Susai Boobalan, M., Venkatesan, P., Ilangovan, A., Kaushik, M.P., Arunagiri, C. Crystallography and computational electronic structure investigations on 14-(3, 4, 5-trimethoxyphenyl)-14H-dibenzo[a,j]xanthene. Journal of Molecular Structure. 2015, 1097, 185-98.

[62] S. Xavier, S. Periandy. Spectroscopic (FT-IR, FT-Raman, UV and NMR) investigation on 1-phenyl-2-nitropropene by quantum computational calculations. Spectrochim. Acta A 149 (2015) 216–230.

[63] M. Chen, U.V. Waghmare, C.M. Friend, E. Kaxiras. A density functional study of clean and hydrogen-covered a-MoO3„010…: Electronic structure and surface relaxation. J. Chem. Phys. 109 (1998) 6854–6860.

[64] K. Fukui. Role of frontier orbitals in chemical reactions. Science 218 (1982) 747–754.

[65] E.R. Johnson, S. Keinan, P. Mori-Sanchez, J. Contreras-Garcia, A.J. Cohen, W. Yang. Revealing noncovalent interactions. J. Am. Chem. Soc. 132 (2010) 6498–6506.

[66] Boobalan, M.s., Ramalingam, S., Amaladasan, M., Tamilvendan, D., Venkatesa Prabhu, G., Bououdina, M. A computational perspective on equilibrium geometry, vibrational spectra and electronic structure of antioxidant active Mannich base 1-[(Pyridin-2-yl amino) methyl] pyrrolidine-2,5-dione. Journal of Molecular Structure. 2014, 1072, 153-72.

[67] M.J. Alam, S. Ahmad. Molecular structure, anharmonic vibrational analysis and electronic spectra of o-, m-, p-iodonitrobenzene using DFT calculations. J. Mol. Struct. 1059 (2014) 239–254.

[68] A.E. Reed, F. Weinhold, Natural bond orbital analysis of near-Hartree–Fock water dimer**.**
J. Chem. Phys. 78 (1983) 4066–4073.

[69] A.E. Reed, R.B. Weinstock, F. Weinhold. Natural population analysis. J. Chem. Phys. 83 (1985) 735–746.

[70] P.K. Chattaraj, B. Maiti, U. Sarkar, J. Phys. Chem. A 107 (2003) 4973–4975.

[71] K. Fukui, Chemical reactivity theory. In: Theory of orientation and stereoselection. Reactivity and structure concepts in organic chemistry, Vol. 2, Springer, Berlin, Heidelberg, 1975.

[72] E. Scrocco, J. Tomasi. Electronic Molecular Structure, Reactivity and Intermolecular Forces: An Euristic Interpretation by Means of Electrostatic Molecular Potentials, Adv. Quantum Chem. 11 (1978) 115–193.

[73] A.J. King. The use of animal models in diabetes research. Br. J. Pharmacol. 166 (2012) 877–894.

Table 1
Geometrical parameters [bond length (Å), bond angle (°) and dihedral angle (°)] of the ICF molecule by B3LYP/6-31G(d, p) method.

Bond length	Theor.	Exp.	Bond angle	Theor.	Exp.	Dihedral angle	Theor.	Exp.
C_1–C_2	1.404	1.347(18)	C_2–C_1–C_6	120.9		C_6–C_1–C_2–C_3	0.0	
C_1–C_6	1.394	1.366(19)	C_1–C_2–C_3	120.9	120.9(14)	C_2–C_1–C_6–C_5	0.0	
C_2–C_3	1.391	1.380(3)	C_2–C_3–C_4	119.1	122.0(13)	C_1–C_2–C_3–C_4	–0.0	
C_3–C_4	1.401	1.415(18)	C_3–C_4–C_5	119.4	119.4(10)	C_2–C_3–C_4–C_5	–0.0	
C_4–C_5	1.416	1.410(13)	C_3–C_4–N_7	124.9		C_2–C_3–C_4–C_7	179.9	
C_4–N_7	1.389	1.340(2)	C_5–C_4–N_7	115.6		C_3–C_4–C_5–C_6	0.0	
C_5–C_6	1.395	1.367(17)	C_4–C_5–C_6	121.4	119.6(10)	C_3–C_4–C_5–S_9	–179.9	
C_5–S_9	1.758	1.718(11)	C_4–C_5–S_9	109.3		N_7–C_4–C_5–C_6	–179.9	
N_7–C_8	1.297	1.285(14)	C_6–C_5–S_9	129.2		N_7–C_4–C_5–S_9	0.0	
C_8–S_9	1.792	1.743(12)	C_1–C_6–C_5	118.1	119.8(10)	C_3–C_4–N_7–C_8	–179.9	
C_8–S_{10}	1.754	1.743(12)	C_5–C_6–S_{28}	121.1		C_5–C_4–N_7–C_8	–0.0	
S_{10}–C_{11}	1.905		C_4–S_7–C_8	111.2		C_4–C_5–C_6–C_1	–0.0	
C_{11}–N_{12}	1.425		N_7–C_8–S_9	115.8		S_9–C_5–C_6–C_1	179.9	
N_{12}–C_{13}	1.485	1.506(17)	N_7–C_8–S_{10}	125.2		C_4–C_5–S_9–C_8	–0.0	
N_{12}–C_{14}	1.477	1.506(17)	S_9–C_8–S_{10}	118.9		C_6–C_5–S_9–C_8	179.9	
C_{13}–C_{20}	1.544	1.519(2)	C_5–S_9–C_8	88.13		C_4–C_7–C_8–S_9	0.0	
C_{13}–C_{24}	1.539	1.518(2)	C_8–S_{10}–C_{11}	99.68		C_4–C_7–C_8–S_{10}	–179.8	
C_{14}–C_{15}	1.540	1.519(2)	S_{10}–C_{11}–N_{12}	110.6		C_7–C_8–S_9–C_5	0.0	
C_{14}–C_{19}	1.546	1.518(2)	C_{11}–N_{12}–C_{13}	114.2		S_{10}–C_8–S_9–C_5	179.9	
C_{15}–C_{16}	1.537	1.525(2)	C_{11}–N_{12}–C_{14}	115.7		N_7–C_8–C_{10}–C_{11}	0.5	
C_{16}–C_{17}	1.536	1.515(3)	C_{13}–N_{12}–C_{14}	119.7	117.8(14)	S_9–C_8–C_{10}–C_{11}	–179.4	
C_{17}–C_{18}	1.535	1.512(3)	N_{12}–C_{13}–C_{20}	110.1	107.6(12)	C_8–S_{10}–C_{11}–N_{12}	178.1	
C_{18}–C_{19}	1.537	1.526(2)	N_{12}–C_{13}–C_{24}	113.5	109.0	S_{10}–C_{11}–N_{12}–C_{13}	107.6	
C_{20}–C_{21}	1.536	1.525(2)	C_{20}–C_{13}–C_{24}	109.0	111.4(13)	S_{10}–C_{11}–N_{12}–C_{14}	–107.4	
C_{21}–C_{22}	1.533	1.515(3)	N_{12}–C_{14}–C_{15}	111.9	107.6(12)	C_{11}–N_{12}–C_{13}–C_{20}	–63.9	
C_{22}–C_{23}	1.533	1.512(3)	N_{12}–C_{14}–C_{19}	114.4	111.2(11)	C_{11}–N_{12}–C_{13}–C_{24}	173.4	
C_{23}–C_{24}	1.539	1.526(2)	C_{15}–C_{14}–C_{19}	110.7	111.4(13)	C_{14}–N_{12}–C_{13}–C_{20}	152.5	178.5(10)
			C_{14}–C_{15}–C_{16}	111.2	110.5(13)	C_{14}–N_{12}–C_{13}–C_{24}	29.9	−59.3(14)
			C_{15}–C_{16}–C_{17}	111.7	111.6(14)	C_{11}–N_{12}–C_{14}–C_{15}	58.9	
			C_{17}–C_{18}–C_{19}	111.5	111.8(14)	C_{11}–N_{12}–C_{14}–C_{19}	–68.0	
			C_{14}–C_{19}–C_{18}	111.5	110.4(13)	C_{13}–N_{12}–C_{14}–C_{15}	–158.1	178.5(10)
			C_{13}–C_{20}–C_{21}	112.3	110.5(13)	C_{13}–N_{12}–C_{14}–C_{19}	74.9	−59.3(14)
			C_{16}–C_{17}–C_{18}	111.2	111.3(15)	N_{12}–C_{13}–C_{20}–C_{21}	178.6	178.6(12)
			C_{20}–C_{21}–C_{22}	111.4	111.6(14)	C_{24}–C_{13}–C_{20}–C_{21}	–56.0	
			C_{21}–C_{22}–C_{23}	110.5	111.3(15)	N_{12}–C_{13}–C_{24}–C_{23}	178.8	−176.3(12)
			C_{22}–C_{23}–C_{24}	112.2	111.8(14)	C_{20}–C_{13}–C_{24}–C_{23}	55.6	−56.4(17)
			C_{13}–C_{24}–C_{23}	111.6	110.4(13)	N_{12}–C_{14}–C_{15}–C_{16}	175.7	178.6(12)
						C_{19}–C_{14}–C_{15}–C_{16}	–55.3	
						N_{12}–C_{14}–C_{19}–C_{18}	–177.2	−176.3(12)
						C_{15}–C_{14}–C_{19}–C_{18}	55.2	−56.4(17)
						C_{14}–C_{15}–C_{16}–C_{17}	55.7	−55.6(19)
						C_{15}–C_{16}–C_{17}–C_{18}	–55.0	54.7(19)
						C_{16}–C_{17}–C_{18}–C_{19}	54.7	−54.7(19)
						C_{17}–C_{18}–C_{19}–C_{14}	–55.0	55.4(18)
						C_{20}–C_{21}–C_{22}–C_{23}	–54.0	54.7(19)
						C_{21}–C_{22}–C_{23}–C_{24}	54.4	−54.7(19)
						C_{22}–C_{23}–C_{24}–C_{13}	–56.3	55.4(18)

Table 2
PES scan of ICF using PM3 method.

Conformer	Coordinates		Energy
	SC–1	SC–2	
C_1	–61.57	–135.68	0.03713
C_2	238.42	–135.68	0.03720
C_3	298.42	–135.68	0.03713
C_4	238.42	224.31	0.03720

Table 3

Vibrational wavenumbers obtained for ICF at B3LYP/6-31G(d, p) method

[harmonic frequency (cm^{-1}), IR intensity ($Kmmol^{-1}$), Raman intensity (arbitrary units)].

Mode	Experimental		Theoretical			TED≥10%	Mode	Experimental		Theoretical			TED≥10%
	FT-IR	FT-Raman	B3LYP	IRint	Ramint			FT-IR	FT-Raman	B3LYP	IRint	Ramint	
1	3426br						31		1560s	1561	2.22	48.09	νCC(67)
2			3109	14.94	14.62	νCH(93)	32			1474	0.81	45.56	βHCH(76)
3			3102	22.43	14.62	νCH(90)	33	1470vs	1469s	1470	8.5	105.39	νCN(72)
4			3092	8.8	69.29	νCH(98)	34			1469	161.34	29.51	βHCH(76)
5		3074ms	3081	1.22	24.37	νCH(96)	35			1460	4.77	5.87	βHCH(69)
6	3055vw		3055	8.17	10.23	νCH(95)	36	1450vs		1456	14.38	4.63	βHCH(70)
7	2999vw	2998vs	2999	78.18	38.42	νCH(78)	37			1454	8.28	9.87	βHCH(68)
8			2998	17.19	56.45	νCH(76)	38			1452	0.89	5.87	βHCH(83)
9			2991	49.52	20.94	νCH(82)	39			1452	2.05	57.71	βHCH(69)
10			2990	4.27	17.2	νCH(89)	40			1450	1.72	59.21	βHCH(69)
11			2981	36.85	32.63	νCH(67)	41			1449	0.61	48.88	βHCH(70)
12			2978	45.71	52.95	νCH(78)	42			1447	16.86	100.25	βHCH(46) + νCC(26)
13			2975	30.46	41.41	νCH(75)	43			1445	0.28	44.98	βHCH(77)
14			2973	42.3	51.2	νCH(77)	44			1438	1.76	22.31	βHCH(53) + τHCSC(10)
15			2972	44.54	89.29	νCH(77)	45			1428	87.16	80.52	βHCC(45) + βCCC(22)
16		2970vw	2971	65.21	109.26	νCH(86)	46	1383vs		1384	1.54	41.21	βHCH(33) + τHCNC(10)
17			2969	62.13	74.37	νCH(83)	47		1364vs	1371	15.25	11.17	βHCH(26) + τCCCC(17)
18	2959vw		2965	49.22	25.83	νCH(78)	48			1351	9.78	16.25	τHCCC(15) + βHCH(10)
19			2941	33.01	56.48	νCH(86)	49			1349	5.83	25.38	τHCCC(13)
20			2940	23.5	13.14	νCH(78)	50			1346	4.43	8.63	τHCCC(15)
21			2930	16.64	15.78	νCH(86)	51			1344	13.96	11.46	τHCNC(25) + τHCCC(14)
22	2924vw		2927	23.95	20.22	νCH(80)	52			1343	2.17	14.28	βHCC(43)
23			2926	24.66	24.93	νCH(87)	53			1338	4.44	9.34	βHCC(41)
24			2924	19.25	24.84	νCH(81)	54			1330	2.43	3.95	βHCC(28)
25			2922	22.58	67.32	νCH(78)	55			1330	6.6	2.34	βHCC(23)
26			2921	21.19	41.41	νCH(87)	56			1327	3.35	9.13	βHCC(40)
27			2919	26.16	50.41	νCH(77)	57	1311vw		1315	7.24	21.76	νCC(71)
28			2917	19.96	48.09	νCH(87)	58		1308w	1309	3.76	10.46	βHCH(53) + τHCSC(10)
29	2817vw	2818vs	2819	44.4	26.85	νCH(99)	59			1307	3.25	24.53	βHCC(37) + τHCCC(14)
30	1588vs		1593	1.59	34.09	νCC(60)	60	1295w		1297	1.69	24.53	τHCNC(33) + τHCNC(15)

Table 3 contd…

Mode	Experimental		Theoretical			TED≥10%	Mode	Experimental		Theoretical			TED≥10%
	FT-IR	FT-Raman	B3LYP	IRint	Ramint			FT-IR	FT-Raman	B3LYP	IRint	Ramint	
61			1273	76.56	22.42	τHCCC(39) + βHCH(14)	91			960	282.34	39.26	βCNC(55) + νCC(12)
62			1264	27.88	39.08	βHSC(17) + νNC(12)	92			950	0.01	0.91	τHCCC(76) + τCCCC(12)
63	1261vw	1263s	1263	4.29	90.15	βHCC(46) + νNC(17)	93			950	1.49	3.4	τHCCC(70) + γSCCC(10)
64			1258	19.33	109.28	βHCC(28) + νCN(15)	94			908	6.85	4.19	νCC(39)
65			1253	3.42	46.02	βHCC(43)	95			901	0.83	15.76	τHCSC(29) + τHCCC(18) + βHCS(10) + νNC(10)
66			1249	1.44	14.18	βHCC(23)	96			895	11.8	4.82	νCC(27)
67			1248	2.86	16.57	βHCC(26)	97			882	7.79	3.18	νCC(56)
68	1241ms		1244	37.4	87.34	βHCC(39)	98			878	0.25	5.92	τHCCC(14) + τCCCC(10) + νCC(10)
69			1230	14.06	21.35	βHCC(29) + τHCCC(11)	99		874vw	877	11.45	14.86	γCCCC(45) + νCC(10)
70			1228	19.91	115.06	νCC(29) + βHCC(26) + νCC(13)	100			871	5.38	6.34	νCC(63)
71			1195	72.35	87.22	βHCC(40)	101			860	11.05	26.74	γHCCC(54) + γSCCC(30)
72		1154s	1168	1.06	4.21	βHCC(23)	102			842	1.96	100.29	βHCS(25) + νNC(21)
73			1148	12.79	38.61	βHCC(58)	103	834w		840	0.45	25.96	τHCCC(77)
74			1148	61.18	51.68	βHCC(15) + τHCCC(10)	104			829	4.91	26.11	νCC(44)
75	1131vw		1132	0.98	8.83	νCN(24)	105		817w	817	0.25	103.67	τHCCC(77)
76	1123s	1121vw	1123	90.63	38.67	βHCC(43) + νCC(17)	106			775	0.21	20.72	τHCCC(29)
77			1111	5.27	109.97	βHCC(48) + νCC(28)	107			771	1.11	18.75	νCC(15)
78			1085	69	31.28	νCN(34) + βHCS(12)	108			767	1.05	19.85	τHCCC(10)
78		1064vw	1065	6.13	6.72	νCC(51)	109	756vs		762	1.58	78.28	νCC(12)
80			1064	10.6	9.19	τCCCC(65) + βNCS(11)	110			745	40.24	9.1	τHCCC(79)
81	1060vw		1061	0.81	0.87	νCC(61)	111	708ms	706w	714	737.95	20.83	γSCCC(49) + τHCCC(29)
82			1055	0.29	8.49	BHCC(35) + τHCCC(18) + τHCNC(13)	112	691ms	690vw	692	6.52	64.97	νSC(25) + βCCN(19)
83	1048s	1042w	1050	21.22	36.93	βCCC(64)	113		678vw	679	74.22	105.79	νSC(24) + βNCS(18) + βCCN(14)
84	1034vw		1035	6.61	41.1	νCC(26)	114	630s	629w	631	5.04	15.72	βCCN(31)
85		1028vw	1028	2.22	40.68	νCC(26)	115			606	1.04	14.94	νCC(34) + βCCN(41)
86			1014	0.22	69.58	νCC(45) + βHCS(12)	116	582s		582	14.92	88.48	τHCCC(65)
87			1012	3.37	61.16	νCC(56) + βHCC(24)	117	567w		578	0.01	4.41	τCCCC(66)
88	998vs	1000vw	1007	5.25	50.54	τHCCC(14) + νCC(17) + βCCC(10)	118			518	30.19	80.67	βCCC(21)
89		986vw	994	7.7	89.35	νCC(20)	119		506w	514	0.06	1.49	τCCCC(65) + τCCNC(15)
90			981	1.98	5.85	βCCC(13)	120		495vw	495	0.03	28.1	βCCC(46) + νSC(16) + βSCC(11)

Table 3 contd…

Mode	Experimental		Theoretical			TED≥10%	Mode	Experimental		Theoretical			TED≥10%
	FT-IR	FT-Raman	B3LYP	IRint	Ramint			FT-IR	FT-Raman	B3LYP	IRint	Ramint	
121			488	0.26	80.67	βCCC(34)	136		235w	240	0.91	9.01	βCNC(18)
122	456s		466	6.09	33.09	βCCC(28) + βCNC(13)	137			228	0.31	17.32	τCCCC(17) + βCNC(10)
123	443vw		444	16.18	35.64	βCCC(30)	138			222	0.03	8.66	τCCCC(19)
124			437	2.01	9.58	βCCC(29)	139			199	0.13	13.66	γCCCN(63) + τCNCC(14)
125			431	1.74	41.14	βCCC(39)	140			185	0.93	52.62	τCCNC(57)
126			423	2.77	1.26	τCCCC(61) + τHCCC(17)	141			157	6.79	61.95	νSC(19) + βCNC(16) + γCCCN(10)
127		407w	408	15.22	81.1	βCCC(12)	142			141	0.9	53.05	τCCCN(33)
128		384vw	389	0.42	66.67	βSCC(34) + νSC(14)	143			111	0.01	75.06	γCCCN(63)
129			369	2.43	15.14	βCNC(16) + βSCC(14) + νSC(14)	144			90	0.8	42.72	τCNCC(40) + βCSC(28)
130			355	6.69	41.58	βCNC(11)	145		76ms	81	0.44	50.06	τCCCN(15) + βCCN(14) + τCNCS(11) + βCNC(11)
131			332	2.64	59.48	βCNC(11)	146			66	1.34	52.96	τCNCS(61)
132		310vw	311	0.77	19.81	τHCCC(14) + βCNC(14)	147			56	0.07	29.07	τCNCC(59)
133			304	2.62	19.46	νCN(33)	148			37	0.72	102.9	τCNCC(14)
134			287	0.01	62.01	τCNCS(73)	149			31	0.12	109.76	τCNCC(47) + τCCCC(15) + βNCS(11)
135			259	0.09	71.08	βCNC(16) + βSCC(12) + νNC(11)	150			21	0.11	11.98	τCSCN(81)
							151			10	0.02	98.74	τCNSC(80)

IR_{int} – IR intensity; Ram_{int} – Raman intensity; br – broad; w – weak; vw – very weak; s – strong; vs – very strong; m – medium; ms – medium strong;

ν – stretching; β – in–plane bending; γ – out–of–plane bending; τ – torsion.

Table 4
Experimental and theoretical ^{1}H and ^{13}C NMR chemical shifts (ppm) of the ICF molecule.

^{1}H NMR				^{13}C NMR			
Atom	δ_{cal}		δ_{exp}	Atom	δ_{cal}		δ_{exp}
	Gas	Solvent	CH_3OH		Gas	Solvent	CH_3OH
H_{25}	7.21	7.58	7.16 (t, *J* = 6.4 Hz, ArH)	C_1	108.6	109.5	123.6
H_{26}	7.33	7.68	7.27 (t, *J* = 6.6 Hz, ArH)	C_2	110.6	111.4	126.4
H_{27}	7.67	7.94	7.57 (d, *J* = 7.1 Hz, ArH)	C_3	106.8	107.0	121.0
H_{28}	7.71	8.01	7.46 (d, *J* = 7.2 Hz, ArH)	C_4	137.3	136.4	148.3
H_{29}	5.74	5.02	3.36 (s, 2H)	C_5	129.7	127.1	136.9
H_{30}	5.06	5.63	3.36 (s, 2H)	C_6	106.1	107.0	122.8
H_{31}	3.21	3.12	3.11–3.10 (m, 2H)	C_8	159.3	162.6	188.3
H_{32}	3.19	3.13	3.11–3.10 (m, 2H)	C_{11}	70.0	60.0	54.4
H_{33}	1.97	1.85	1.80–1.78 (m, 8H)	C_{13}	57.6	52.0	64.8
H_{34}	2.07	1.85	1.80–1.78 (m, 8H)	C_{14}	52.9	47.3	64.8
H_{35}	2.01	1.88	1.90–1.88(m, 8H)	C_{15}	30.0	25.2	31.2
H_{36}	1.58	1.56	1.90–1.88 (m, 8H)	C_{16}	24.3	19.1	25.7
H_{37}	1.41	1.35	1.90–1.88 (m, 8H)	C_{17}	23.1	18.0	26.3
H_{38}	1.70	1.63	1.77–1.66 (m, 4H)	C_{18}	22.8	17.7	25.7
H_{39}	1.89	1.79	1.90–1.88 (m, 8H)	C_{19}	23.9	19.3	31.2
H_{40}	1.49	1.47	1.90–1.88 (m, 8H)	C_{20}	31.6	26.8	31.2
H_{41}	1.69	1.62	1.80–1.78 (m, 8H)	C_{21}	22.2	17.3	25.7
H_{42}	1.82	1.79	1.80–1.78 (m, 8H)	C_{22}	23.0	17.9	26.3
H_{43}	1.37	1.22	1.80–1.78 (m, 8H)	C_{23}	23.2	18.1	25.7
H_{44}	2.61	2.42	1.80–1.78 (m, 8H)	C_{24}	28.1	23.1	31.2
H_{45}	1.93	1.82	1.90–1.88 (m, 8H)				
H_{46}	1.58	1.53	1.90–1.88 (m, 8H)				
H_{47}	1.45	1.40	1.77–1.66 (m, 4H)				
H_{48}	1.75	1.67	1.90–1.88 (m, 8H)				
H_{50}	1.59	1.53	1.90–1.88 (m, 8H)				
H_{51}	1.39	1.33	1.80–1.78 (m, 8H)				
H_{52}	2.11	2.08	1.80–1.78 (m, 8H)				

Table 5
Experimental and calculated absorption wavelength (λ, nm), energies and oscillator strength (f) of ICF using the TD-DFT method at B3LYP/6-31G(d, p) method.

Excitation	CI expansion coefficient	Cal. Gas phase	f	Excitation	CI expansion coefficient	Cal. DMSO	f	Exp.	Assign.	In solvent [a]Major contribution (≥10%)
Excited state 1										
96→98	0.4498	282	0.0069	97→98	0.7012	292	0.0047	326	n→π*	H→L (98%)
97→98	0.5377									
Excited state 2										
95→98	0.2385	271	0.3548	95→98	–0.1685	275	0.5154		n→π*	H-1→L (86%)
95→99	0.1293			95→99	–0.1685					H-2→L (6%)
96→98	0.4823			96→98	0.6558					H-2→L (2%)
97→98	–0.3928			97→100	0.1107					H→L+2 (2%)
97→99	0.1032									
Excited state 3										
95→98	0.3589	261	0.0722	95→98	0.5124	261	0.0972		π→π*	H-2→L (53%)
96→99	–0.1574			96→99	0.1877					H-1→L+1 (36%)
96→99	–0.2308			96→99	0.4247					H-1→L (7%)
96→100	–0.2649									
97→98	0.1300									
97→99	0.2537									
97→100	0.3568									

[a] H – HOMO; L – LUMO.

Table 6
Experimental and simulated energy gap of ICF molecule.

Experimental		B3LYP-31G(d, p)					
Solvent phase		Solvent phase			Gas phase		
λ_{max} (nm)	Energy gap (eV)	λ_{cal} (nm)	Energy gap (eV)	Energy (cm^{-1})	λ_{cal} (nm)	Energy gap (eV)	Energy (cm^{-1})
326	3.14	282	4.40	35511.22	292	4.24	34210.24
		271	4.58	36932.38	274	4.52	36433.12
		261	4.6	38379.35	261	4.74	38259.17

Table 7
HOMO, LUMO, energy gap, global electronegativity, global hardness and softness, global electrophilicity index and dipole moment of the ICF molecule.

Parameters	B3LYP/6-31G(d, p) (eV)	
	Gas phase	Solvent phase (DMSO)
HOMO	–5.69	–5.72
LOMO	–0.68	–0.85
$\Delta E_{HOMO} - \Delta E_{LUMO}$ gap	–5.01	–4.87
Ionization potential (I)	5.69	5.72
Electron affinity (A)	0.68	0.85
Chemical potential (μ)	–3.19	–3.28
Chemical hardness (η)	2.51	2.44
Electronegativity (χ)	3.19	3.28
Softness (σ)	0.40	0.41
Electrophilicity index (ω)	12.77	13.13
Dipole moment (Debye)	2.1974	2.4979
SCF Energy (Hartrees)	2352.3791	2352.3791

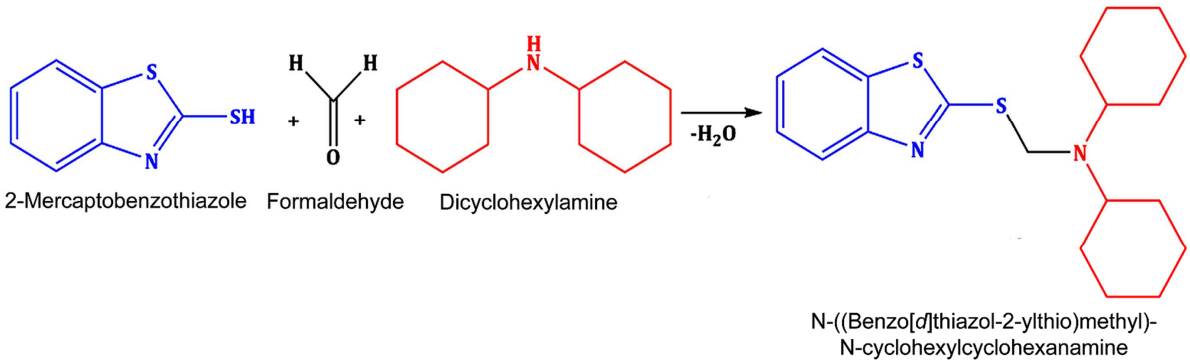

Fig. 1. Synthesis of N-((benzo[*d*]thiazol-2-ylthio)methyl)-N-cyclohexylcyclohexanamine (ICF).

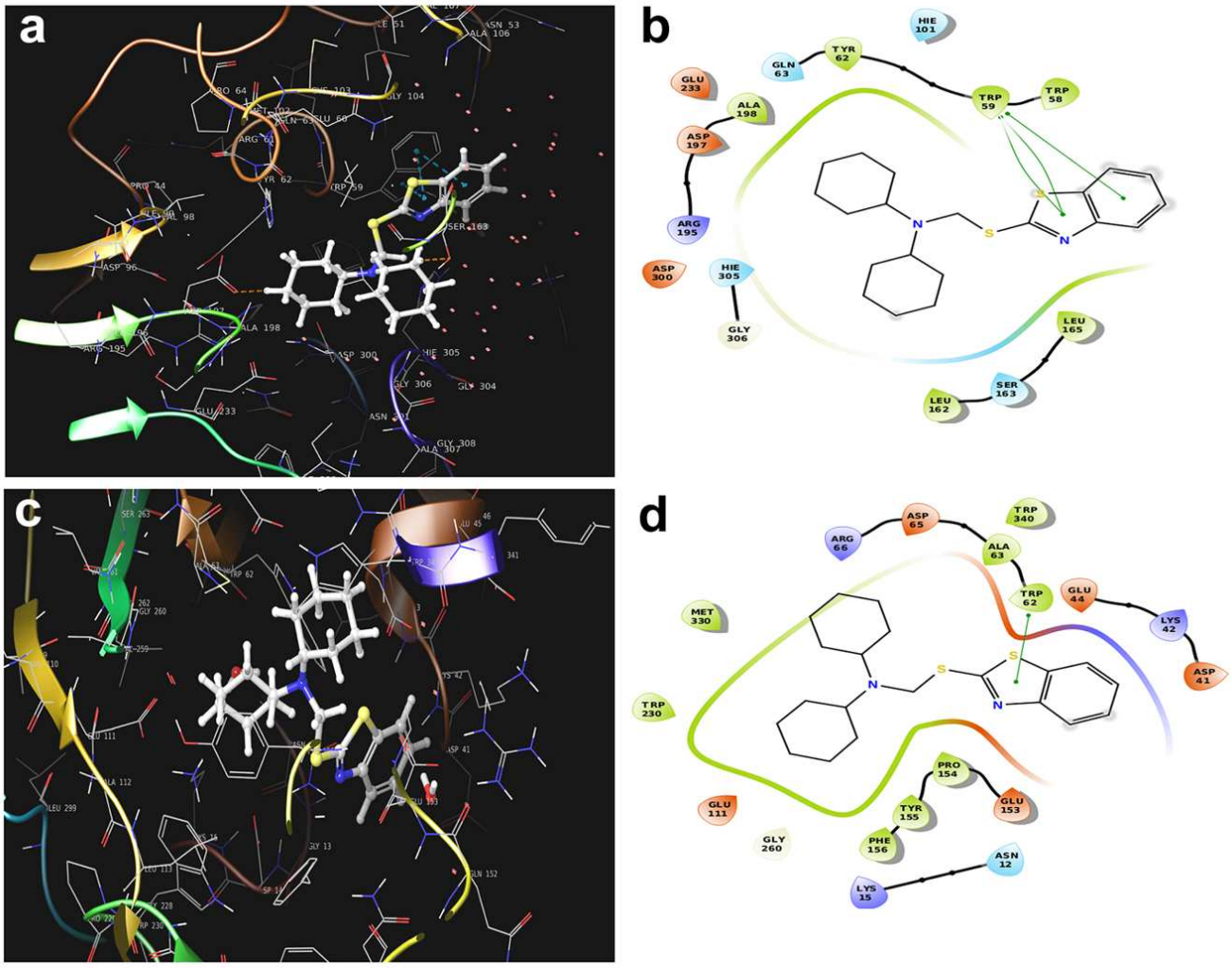

Fig. 10. The binding site of ICF molecule with 1Z32 and 3G7V protein of a,c) 3D and b,d) 2D structure.

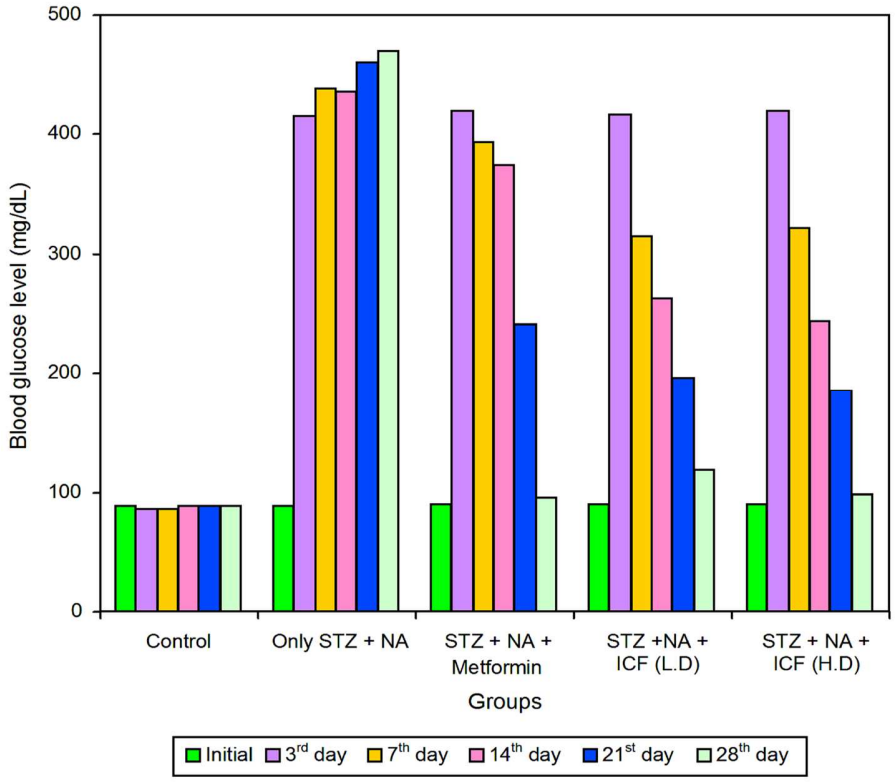

Fig. 11. Effect of ICF molecule on fasting blood glucose level in diabetic rats.

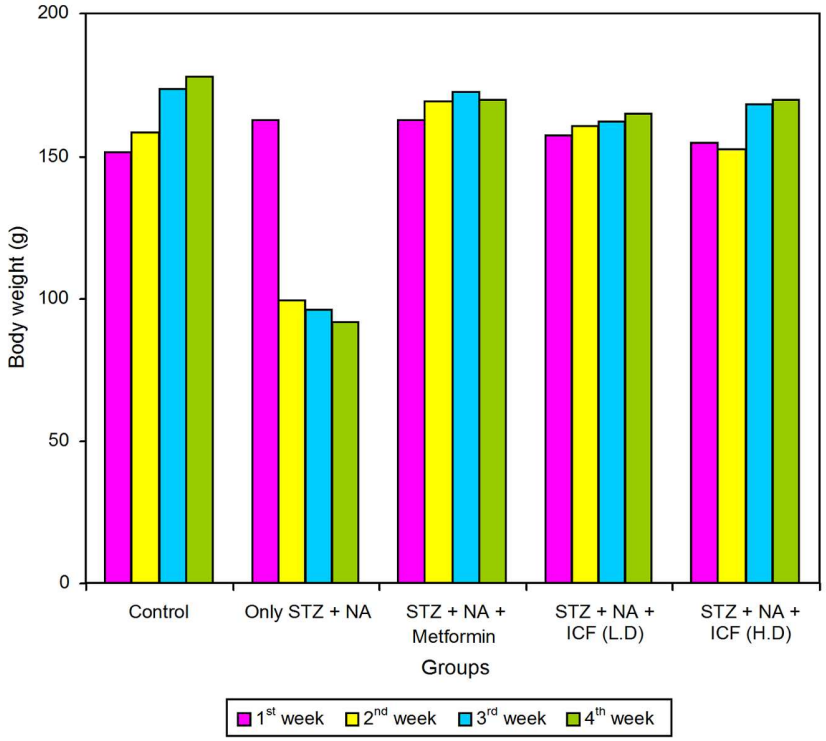

Fig. 12. Effect of ICF molecule on fasting body weight in diabetic rats.

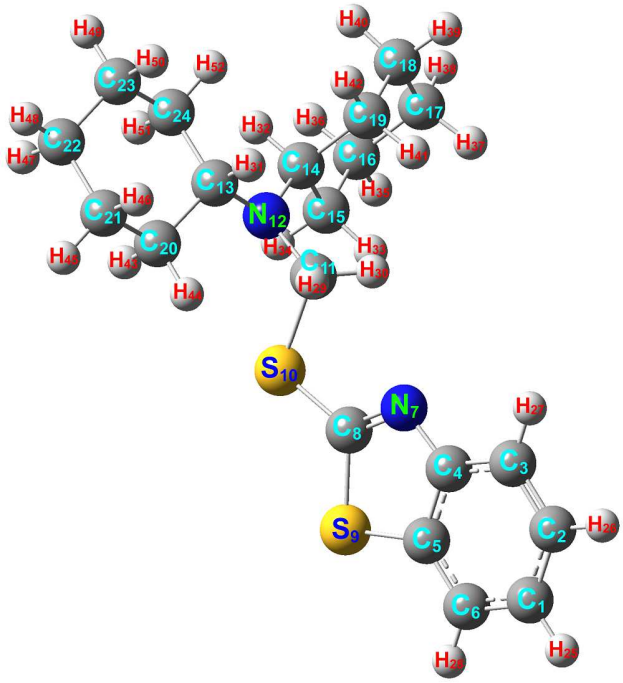

Fig. 2. Optimized geometry of ICF molecule.

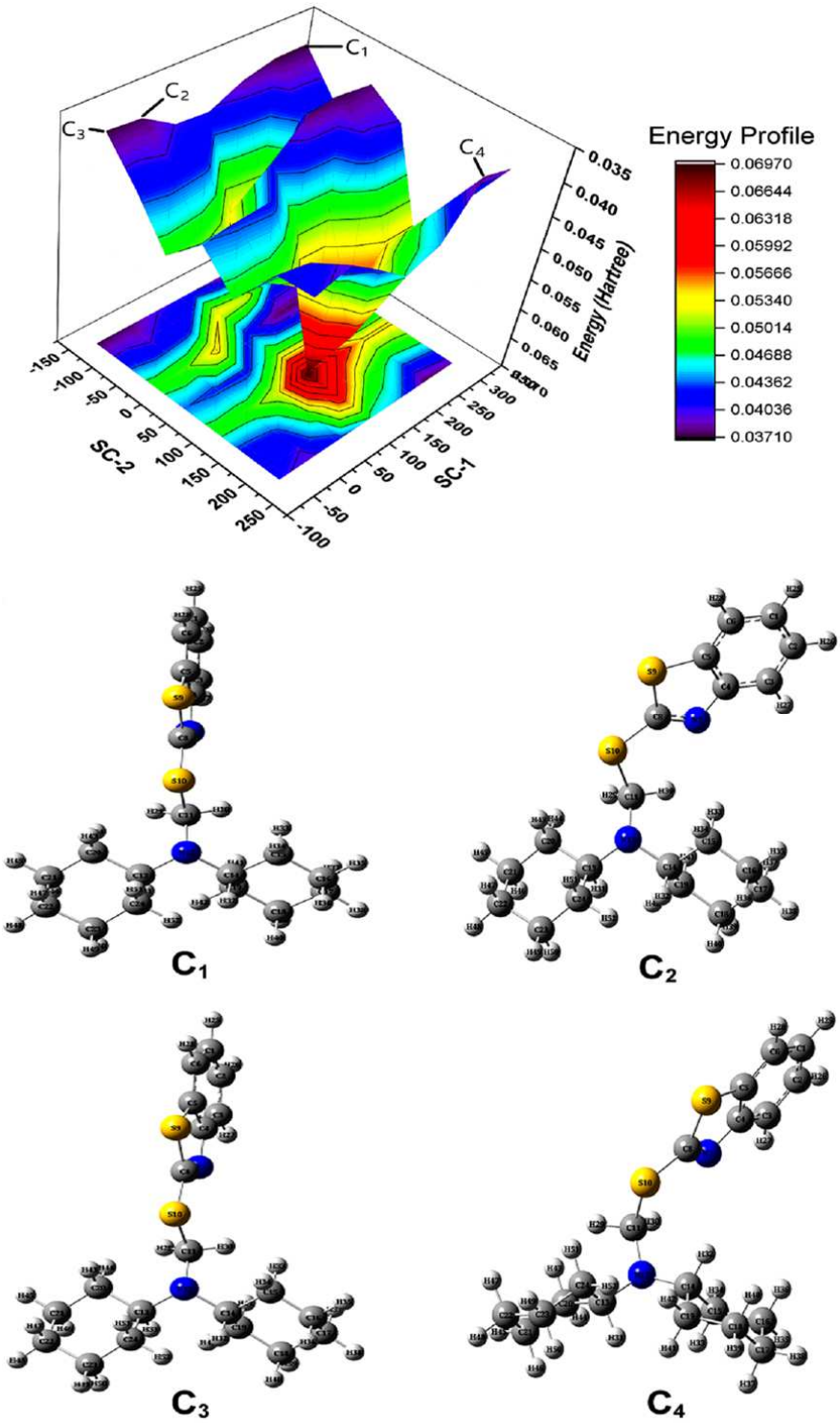

Fig. 3. The PES scan, conformers and energy profile of ICF using PM3 method.

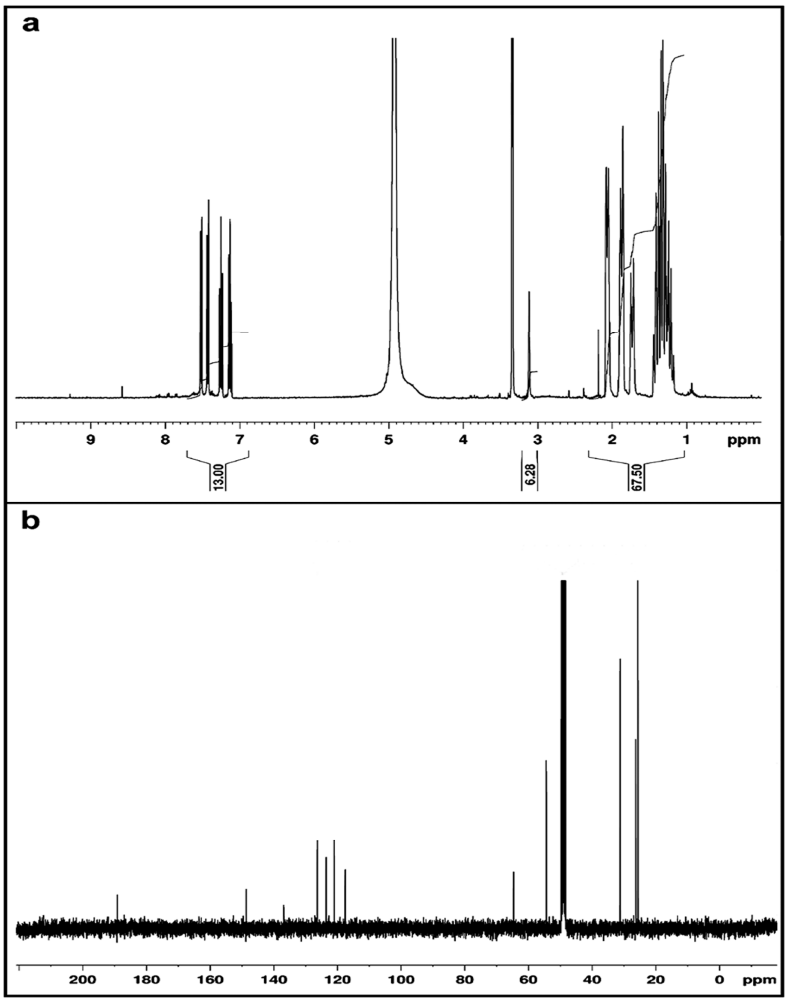

Fig. 4. a) ^{1}H and b) ^{13}C NMR spectra of ICF molecule.

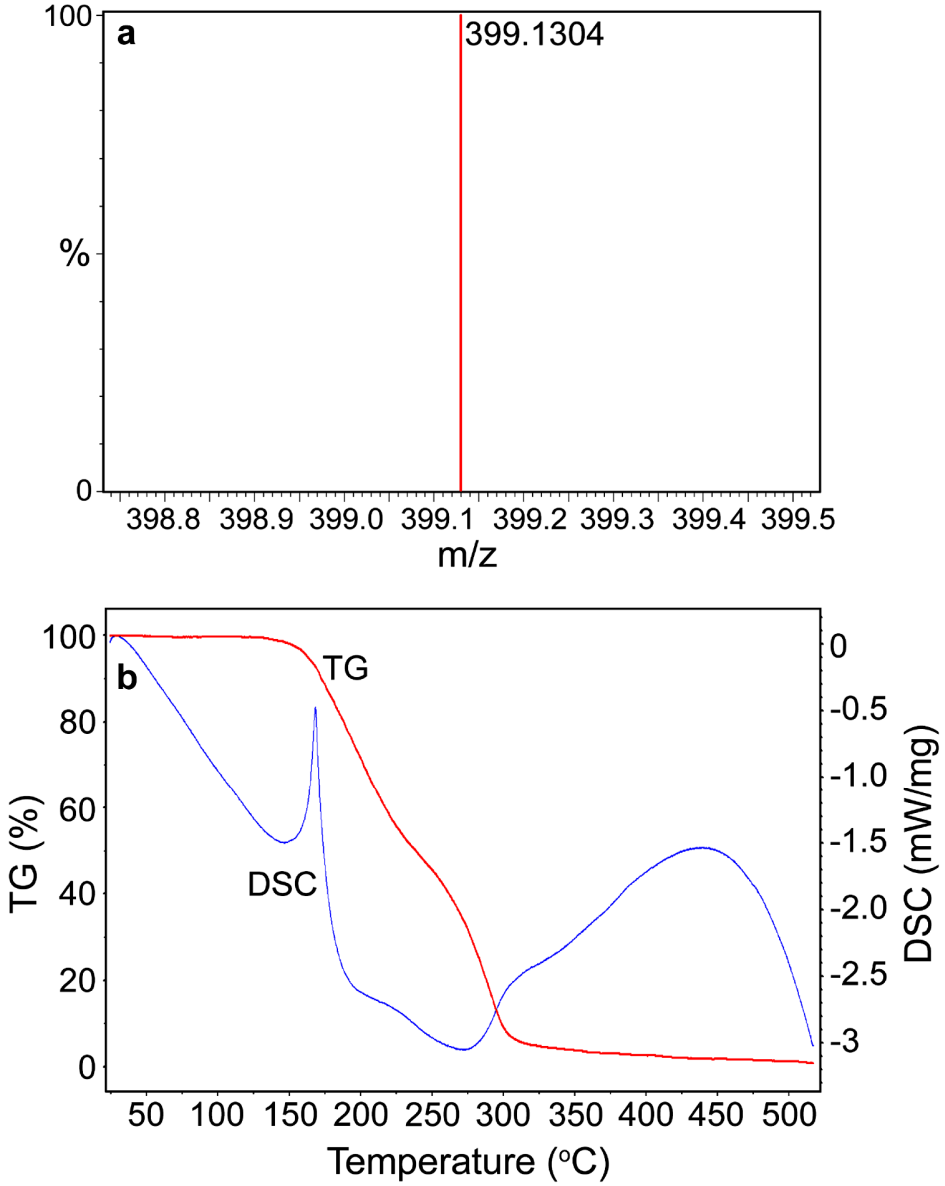

Fig. 5. a) Mass spectrum and b) TG/DSC curves of ICF molecule.

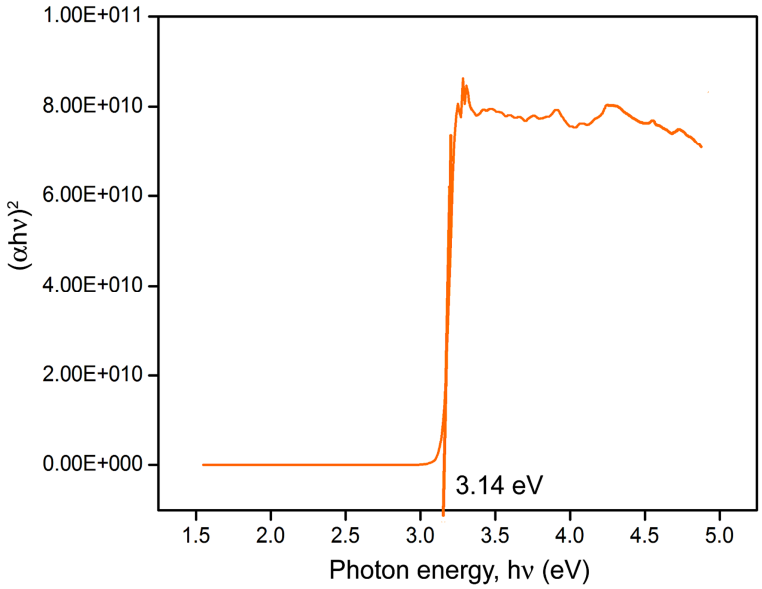

Fig. 6. Plot of $(\alpha h\nu)^2$ *Vs* $h\nu$ (eV) for determining energy gap of ICF molecule.

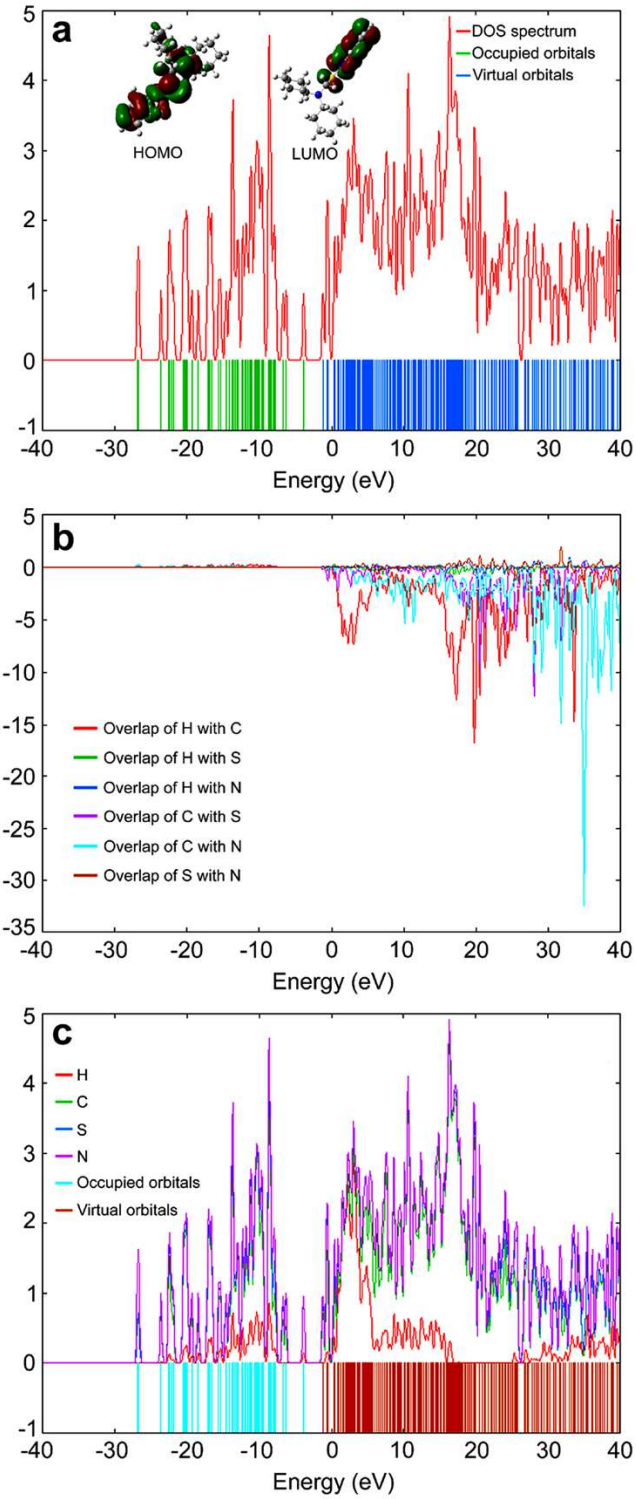

Fig. 7. a) HOMO-LUMO, DOS, b) OPDOS and c) PDOS diagrams of ICF molecule.

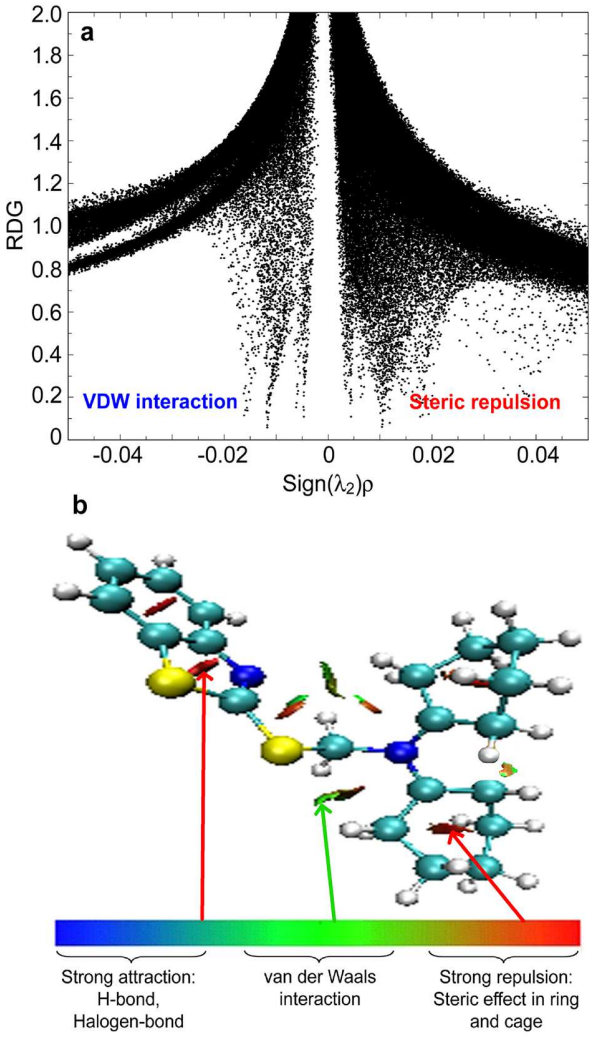

Fig. 8. a) The reduced density gradient and b) coloured surface of ICF molecule.

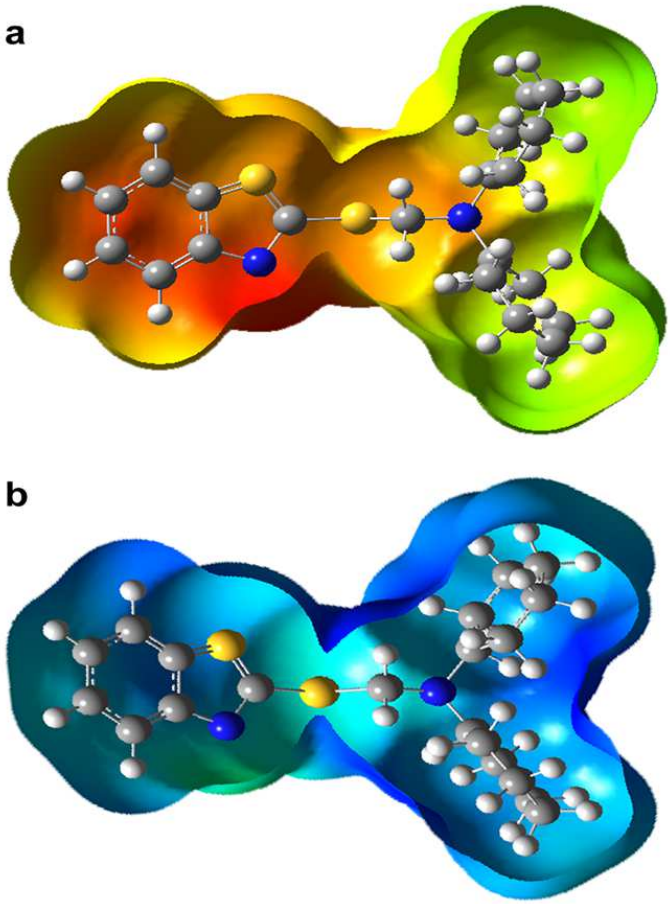

Fig. 9. Fukui function: a) f^{+} and b) f^{-} of ICF molecule.

Research Highlights

- Molecular structure, spectra (UV-Vis, vibrational, NMR, HRMS) and electronic structure of new Mannich base has been investigated and compared by experimental results with DFT Computing.
- Significant molecular docking score has been observed against diabetic protein 1Z32 and 3G7V.
- Anti-diabetic evaluation performed using in vivo, effect of blood glucose level and body weight was examined. Significant *in vivo* were results observed.

Declaration of interest statement

We wish to confirm that there are no known conflicts of interest associated with this publication and there has been no significant financial support for this work that could have influenced its outcome.